Nanofibrous and Laminated Nanocomposites:

Manufacturing and Characterization

by

FARZIN JAVANSHOUR

Submitted to the Graduate School of Engineering and Natural Sciences

in partial fulfillment of

the requirements for the degree of

Master of Science

Sabanci University

AUGUST 2017

Nanofibrous and Laminated Nanocomposites:

Manufacturing and Characterization

APPROVED BY:

Assoc. Prof. Dr. Melih Papila (Thesis Supervisor) ....

Prof. Dr. Ali Rana Atılgan ....

Asst. Prof. Dr. Elif Özden Yenigün ....
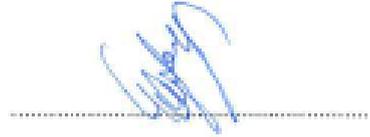
DATE OF APPROVAL: 01/08/2017

Important thing in science is not so much to obtain new facts as to discover new ways of thinking about them.

Sir William Bragg

.

to my family...

ACKNOWLEDGEMENTS

Nanofibrous and Laminated Nanocomposites:

Manufacturing and Characterization

FARZIN JAVANSHOUR

M.Sc. Thesis, August 2017

Thesis Advisor: Assoc. Prof. Melih PAPILA

Keywords: Nanofibers, Nanocomposite, Laminate, Mechanical Behavior, Electrospinning

ABSTRACT

Electrospun nanofibers are proven to be effective toughening agents in polymer matrix composites. They are typically incorporated into laminated composites as interlayers such that resistance against delamination and progression of matrix cracking through the thickness are enhanced in comparison to the neat resin dominated interlaminar characteristics. The nanofibrous interlayers are indeed nanofiber reinforced nanocomposites. This thesis work presents an approach for manufacturing nanocomposites which are representative of the in-situ interlayer formation during the cure and consolidation of the prepreg based laminated composites. Several nanofibrous veils of different base polymers are studied. Mechanical and thermal characterization of the nanofibers and their epoxy matrix nanocomposites are reported along with the reference results on neat epoxy. Scalability of the nanocomposites is also demonstrated by processing novel nanofiber/epoxy laminated nanocomposites much like forming structural laminates. The proposed manufacturing approach enables to collect representative and consistent nanocomposite mechanical test data. The material model and the elastic modulus of single nanofibers are back calculated in reference to

experimental tensile behavior of the neat epoxy and representative nanofiber/epoxy nanocomposites. The results are compared with the elastic moduli of single nanofibers extracted with Atomic Force Microscope (AFM) reported in the literature.

Nanofiber Destekli ve Laminat Nanokompozitler:

Üretim ve Karakterizasyon

FARZIN JAVANSHOUR

ÖZET

Elektrodokunmuş nanoliflerin, polimer matriks kompozitler için etkin toklaştırıcı dolgular/güçlendiriciler olduğu kanıtlanmıştır. Çoğunlukla reçine-zengin olan bölgelerin özellikleri dikkate alındığında, nanolifli kompozit malzemelerde delaminasyona karşı direnç artışı ve matris kırılmalarının geciktirilmesi özelliklerinin iyileştirildiği gözlenmiştir. Nanolifli (nanofibrous) arayüzeyler/arakatlar aslında nanolif takviyeli nanokompoziterlerdir. Bu tez çalışması prepreg bazlı lamine kompozitlerin kürlenme ve konsolidasyonu sırasında arakat nanokompozitlerin oluşumunu gerçekçi temsil eden bir üretim yaklaşımı sunmaktadır Farklı baz polimerlerin elektrodokunmuş nanolifli matları bu yaklaşım ile incelenmiştir. Nanoliferlerin ve epoksi matriks nanokompozitlerinin mekanik ve termal olarak karakterize edilmesi, takviyesiz epoksi üzerindeki referans sonuçları ile birlikte rapor edilmektedir. Ayrıca nanokompozit yaklaşımının ölçeklenebilirliğini göstermek amacıyla, yapısal laminat kompozitlerin üretimine benzer, nanolif/epoksi laminat nanokompozitler üretilmistir. Önerilen üretim yaklaşımı, temsili ve tutarlı nanokompozit mekanik test verilerini toplamayı sağlamaktadır. Tek nanolif malzeme model ve elastik modülü, saf epoksi ve temsili nanofiber/epoksi nanokompozitlerin deneysel çekme/gerilme davranışına referansla geri hesaplanmıştır. Sonuçlar, literatürde raporlanmış Atomik Kuvvet Mikroskopu (AFM) ile çıkarılan tekli nanoliflerin elastik modülü ile karşılaştırılmıştır.

LIST OF FIGURES

vii

LIST OF TABLES

List of Contents

CHAPTER 1

GENERAL INTRODUCTION

1.1. Nanofibers: Processing Techniques and Potential Fields of Application

Nanofibers with high surface area to volume ratio, aligned macromolecular chains, reduced probability of finding flaws along the surface area, high aspect ratio are desirable in numerous applications. Despite the variety of nanofiber manufacturing methods in the literature such as melt spinning [1], chemical vapor deposition [2], gas jet[3], self-assembly[4], significant amount of research studies in the literature have been dedicated to electrospinning technique due to high throughput, operational simplicity, and low cost[5]. Electrospinning phenomena discovered by Sir William Giblert (1628) [5]. Formation of fiber from entangled droplet of viscous polymer driven by applied electrical field known as "Taylor Cone" was later studied, and mathematically formulated by Sir Geoffery Taylor (1960) [6]. As depicted in Figure 1A, the basic mechanism of the electrospinning could be described as polymer solution forced by an electrostatic force through a hollow needle (or any surface capable of forming Taylor cone) while an electric field is typically applied between the needle (or other types of electrode) charged by high voltage and grounded conductive surface/collector (e.g. a metal plate). Researchers have studied formation of the Taylor cone [7,8] and controlling parameters (e.g. feeding rate [9], filed strength [10,11], distance between the electrode and collector [12], humidity [8], viscosity [13] and molecular weight [14] of polymer) as it is crucial to maintain a stable electrospinning process as such affects resultant morphology of the spun nanofibers and their mats [8]. Electrospinning technique could be categorized as needle based and needleless methods. Needle based technologies for mass nanofiber production such as BioInicia [15] can precipitate polymer at the needle tip as such needle blockage is typically the main challenge against continuous jet flow [5]. Roller electrode based spinning as a needless approach developed by Jirsak et al [16], commercially named as Nanospider has solved the spinning drawbacks of needle based electrospinning. It provides higher productivity

which is needed for mass production and industrial scale application of nanofibers in the (e.g. filtration, textile, composites) Figure 1B. Leading material companies optimize the electrospinning techniques in terms of productivity, production rate, profitability, and environmental issues [5]. For instance, Revolution Fibers Ltd [17] has developed a needleless spinneret with control over Taylor cone for by eliminating common problems in the needle-based and free surface electrospinning [5]. Elmarco [18] as another leading company in the electrospinning technology has devised a novel needleless technique as coated wires are utilized as spinneret. Their high performance products are customized for specific applications such as Xantulayer [17] nanofibrous veil developed by Revolution Fibers as the world's first commercial composite reinforcement product with outstanding mechanical properties such as improvement in fatigue life of composites up to 400% [19].
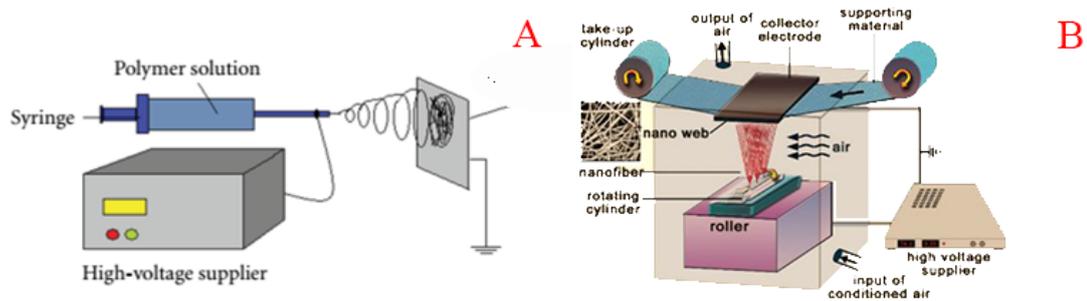
Figure 1 Schematic view of electrospinning technique. A: needle based spinning B: roller spinning (Nanospider).

1.2. Electrospun nanofibers as toughening interlayers in structural composites

Growing applications of laminated composites in key engineering disciplines and design problems set prominence to interlaminar toughness and strength [20]. Because interlaminar failure mechanisms are among the most dominant failure modes [21] (specifically under impact and fatigue loading [22–24]). Interlaminar region known as the region between two subsequent plies is typically comprised of the matrix phase and

responsible from effective load transfer between the subsequent composite plies without damage initiation and progression. Processed (cured) laminated composite plies under exerted loads do not necessarily have identical expansion or contraction response as the fiber orientation may vary in each ply by design [21]. This makes interlaminar region susceptible to interlaminar stresses, which may lead to crack initiation and premature damages. To enhance delamination and through the thickness crack resistance of the composites, various techniques have been developed over the years such as optimization of stacking sequence [25–29], laminate stitching [30], and critical ply termination [31]. However, these methods might adversely affect other properties of the composite. An alternative trend is addition of macro or nano-scale particles [32,33] into the epoxy matrix or inserting tough polymer films [27] into the interlaminar regions. Main draw backs of the particle toughened epoxy systems are uneven dispersion of particles, adverse increase in viscosity of epoxy matrix for out of autoclave composite manufacturing systems, and degradation of in plane stiffness and strength [34,35]. Furthermore, film interleaving could be unsuitable for resin transfer molding systems as it could intervene resin flow and cause poor fiber-matrix adhesion [36] and could adversely affect stiffness design in prepreg based systems [35]. Electrospun nonwoven nanofibrous mats as an alternative interlaminar toughening agent with nanoscale fiber diameter could be incorporated in a thin matrix rich interlaminar region like "hooks and loops" in Velcro[21,37]. This novel technique, first proposed by Dzenis Y, Reneker [37–39] was later studied by numerous researchers proving the efficiency by the use of different base polymers and matrix systems according to various applications. Some of these developments are reported in Table 1. Significant improvement in the interlaminar fracture toughness, impact resistance, and delamination strength addressed by electrospun nanofibrous veil interleaved in the interlaminar region interpret the importance of this toughening technique.

The thin resin rich interlaminar region reinforced with electrospun nanofiber mats is effectively a nanofiber reinforced nanocomposite by itself. This gives prominence to the need for development of effective and representative nanofibrous nanocomposite manufacturing systems, much like the nanofiber/epoxy layer in the interlaminar region

7

with same resin type and nanofiber-matrix configuration. Such an effective representative nanocomposite and its characterization may provide representative data that is essential for better interlaminar toughening design and a conceptual way to predict reinforcing capabilities of nanofiber mats can be devised. For instance, this approach could be enabling in development of better representative volume element (RVE) and material models for laminated composites within Finite Element method as such mechanical properties of single nanofiber which is hard to test could be extracted by the back calculation strategies utilizing measured mechanical properties of neat sample and nanofiber reinforced nanocomposite.

Table 1 Selected list of composite systems interleaved with nanofiber veils from the literature.

Author/ Year	Fiber / matrix	Nanofibrous Interlayer	Experiments	Improvement (%)
Bilge et al., 2012 [40]	Carbon/Epoxy	P(St-co-GMA)	3PB	Flexural Strength 16%
			ENF	G_{IIC} 55%
			Impact	Absorbed energy 8%
			TT	Transverse tensile strength 17%
		P(St-co-GMA)/MWCNT	3PB	Flexural Strength 16%
			ENF	G_{IIC} 55%
			Impact	Absorbed energy 8%
			TT	Transverse tensile strength 17%

Table 1 (continued)

8

Author/ Year	Fiber / matrix	Nanofibrous Interlayer	Experiments	Improvement (%)
Bilge et al., 2017 [41]	Carbon/Epoxy	P(St-co-GMA)	Split Hopkins Pressure Bar	In plane Ultimate Compressive Strength 80%
				Through the Thickness Ultimate Compressive Strength 40%
Beckermann et al., 2015 [35]	Carbon/Epoxy (Prepreg)	PA66 (4.3 g/m2)	ENF & DCB	G_{IC} 156% G_{IIC} 69%
		PVB (4.3 g/m2)		G_{IC} 53% G_{IIC} -6%
		PA66 (9g/m^2) /PVB		G_{IC} -33% G_{IIC} 45%
Daelmans et al., 2017 [23]	Carbon/Epoxy (Prepreg)	PA6	ENF & CCP	$G_{IIc, CCP}$ 28% $G_{IIc, ENF}$ 30%
		PA6.9	ENF &CCP	$G_{IIc, CCP}$ 31% $G_{IIc, ENF}$ 46%
		PCL	ENF & CCP	$G_{IIc, CCP}$ 25% $G_{IIc, ENF}$ 41%
Heijden et al., 2014 [42]	Glass/Epoxy (RTM)	PCL	DCB	G_{IC} 100%

Table 1 (continued)

Author/ Year	Fiber / matrix	Nanofibrous Interlayer	Experiments	Improvement (%)
Heijden et al., 2017 [43]	Glass/Epoxy (VARTM)	0.4 % cross-linked SBS	ENF & DCB	G_{IIc} -29%
		5.45% cross-linked SBS		G_{IIc} 100%
		0.65- 1.5% cross-linked SBS		G_{Ic} 80-90%
Brugo et al., 2016 [44]	Carbon/Epoxy UD (Prepreg)	PA6.6 , mat thickness: 40μm and 90 μm	ENF & DCB	G_{Ic40} 57%, G_{IIc40} 61%, G_{Ic90} 48%, G_{IIc90} 62%
	Carbon/Epoxy Plain Wave (Prepreg)			G_{Ic40} 131%, G_{IIc40} 40%, G_{Ic90} 250%, G_{IIc90} 147%
Nash et al., 2014	Benzenoxazine 9120 (VARTM)	Nylon	3PB, DCB	Flexural Modulus - 15% G_{Ic} 80%
Saghafi et al., [45]	Glass/Epoxy (Prepreg)	PAN	Low Velocity Impact (weight drop)	Absorbed Energy - 6.6 %
Bilge et al., 2014 [46]	Carbon/Epoxy	P(St-co-GMA)	T	Ultimate Tensile Strength 12%
			OHT	Open Hole Tensile Strength 9%

1.3. Critical Review on the Processing Methods of Structural Nanocomposites

Polymeric nanocomposites have drawn a great deal of attention and numerous studies have been reported in the literature which also include composites incorporating nanofibers. Thanks to the nanoscale enabled characteristics such as high surface area, material properties can be tailored and improved at the macro-scale given an effective choice of nanocomposite making strategy. In reference to various polymeric systems and desired applications, nanocomposite manufacturing techniques could be divided into infiltration based production methods including solution mixing and casting [47,48], wetting and stacking [49], and methods other than infiltration such as compression molding [50–54]. Specific to the electrospun nanofibrous mats as embedded into the polymer matrix which is also the focus of this work, research-studies can be noted [50–54]. In nanocomposite processing techniques where viscous polymer flow is needed, e.g. when high viscous solution poured in mold, air can be trapped leading to voids which are potential to cause premature failure [55,56]. Another well-known major issue is the difficulties of effective dispersion of the nanoscale fillers. Homogeneous dispersion of nano-fillers as a crucial need for enhanced properties could be partially achieved with combination of ultrasonic treatment, use of nonionic surfactants, and high-speed mechanical stirring [55–57]. Rana et.al [57] for instance, reported minimum agglomeration of 0.1% CNF and 0.2% nonionic surfactant by weight in epoxy resin after 2h of ultrasonication, but large agglomeration in the case of 0.5% CNF. Higher percent of surfactant resulted in decreased storage modulus (E') of the samples. Although higher acetone concentration altered dispersion of the nanotubes, glass transition temperature (T_g) and storage modulus (E') of the samples were deteriorated [58]. Mechanical stirring could harm the fillers and deteriorate properties of the nanocomposite [55].

Electrospun continuous nanofiber mats could be advantageous over particles and short fibers as also discussed in the previous part. They can overcome

agglomeration problems which is a common issue in nano-filler added solution casting based methods [50,55–59]. Higher stiffness as a result of inherent interconnecting nature of electrospun networks, and high aspect ratio of the nanofibers are also expected [21,60]. It was reported that they could arrest propagation of micro cracks as a result of micromechanical interlocking [50].

Nanofibers as reinforcing agents of nanocomposites could be directly spun onto the matrix polymer solution [49] or other reinforcing media such as fabrics [49,61]. Jiang et al. [49] proposed a manufacturing method for nanofiber reinforced laminated thermoplastic matrix composite with layer by layer procedure. They casted solution of 1mL 2.5 wt% thermoplastic polyurethane (TPU) in DMF on a glass die, electrospun one thin layer of nylon-6 onto it and dried at 100°C. These steps were repeated to additively achieve desired configuration and thickness. Moreover, electrospun nanofibrous mats as a self-supporting veils could be stacked together and impregnated in the polymer matrix to form nanocomposites [51,52,60]. Ozden et al. [51] for instance cut MWCNTs/P(St-co-GMA) fiber web into 12mm × 50mm pieces and embedded 10 layers of them layer by layer into epoxy resin in a Teflon mold. The epoxy matrix nanocomposite specimens were cured at 50°C for 15 h, and post cured at 80°C for 48h.

1.4. Proposed Approach on the Processing Methods of Nanocomposites as Interlayers for Structural Composites

In this thesis an alternative nanocomposite processing with the electrospun nanofibers is proposed to better represent in-situ nanofibrous nanocomposite formation in the interlaminar region of structural laminated composites (thin nanofibrous veil embedded resin rich area). The method can be considered as a

novel adaptation of resin film infusion methodology into nanocomposites. It is also demonstrated as an effective way to fabricate nanofiber reinforced laminated nanocomposites. The methodology enables controlled and homogenous distribution of the reinforcing nanofibrous mats as nanocomposites constituents (resin film and electrospun nanofiber mat) are stacked like in case of prepreg lay-ups. It is a single-step cure process following the lamination of resin film layers and electrospun nanofibrous mats. As the shape and the thickness (or configuration) of the processed nanocomposites are conveniently tunable, various mechanical tests could be performed in the assessment of reinforcing and toughening characteristics of nanofibrous mats. For instance, tension test with Dynamic Mechanical Analysis (DMA) which is not commonly applicable by the previous manufacturing techniques. More on the advantages, the proposed nanocomposite processing technique could (ideally) employ the resin film which is identical to the prepreg resin system of interest for laminated composite. This provides an opportunity in assessment of the reinforcing capabilities of the nanofibrous veils embedded in the same resin film as the prepreg system by itself, better representing their in-situ toughening performance as interlayer in structural composites.

In this research work, commercially available epoxy resin film and nanofibrous veils based on different base polymers are used in order to highlight the scalability of the approach and associated nanocomposites. Properties of the nanofibrous reinforcement are first characterized. These include morphology of the mats as is and after exposure to the curing temperature of epoxy by Scanning Electron Microscope (SEM), fiber mat wettability (Contact angle measurement), and mechanical properties under tension by universal testing machine (UTM). Next, following the proposed application of the laminated nanocomposite processing method superior flexural strength (by UTM) and tensile strength (by UTM and DMA) are sought among the selection of fibers types in comparison to the neat resin mechanical performance. In-situ behavior at mechanical loading, that is load transfer and interaction between the fiber and epoxy matrix are

discussed via fracture surface analyses (using SEM images). Moreover, physical properties of a single nanofiber in an electrospun nanofibrous mat such as modulus and material model could be extracted by back calculating (with FEA) the experimental data of neat resin samples and nanocomposites manufactured by the proposed resin film infusion approach.

1.5. Thesis Structure

Six inter-connected chapters constitute this thesis work. The first chapter as presented is the general introduction on nanofibers and their toughening potential with specific emphasis on the electrospun nanofiber mats, processing methods of nanocomposites, a novel processing technique of nanocomposites as interlayers in structural composites followed by their advantages and coming by opportunities. The second chapter is methodology. The third chapter is an assessment on various polymeric nanofibers as nanocomposites reinforcement. The fourth chapter is a discussion on the scalability potential of the proposed resin film infusion technique in process of nanofiber/epoxy laminated nanocomposites. In the fifth chapter mechanical properties and material models for single nanofibers of PA6, PAN, PVB, and Xantulayer nanofibrous mats is extracted based on FEA by back calculating the experimental results of neat resin samples and nanocomposites which is a part of TUBITAK funded project "Integration of nanocomposite interlayers into structural composites for higher fracture toughness and strength," no 213M542. The last chapter includes future works and equations employed in the back calculating process in Digimat-MX.

The contents of these chapters are formed of one unpublished under review journal article submitted to Composites Science and Technology "**Synergistic role of In-Situ Crosslinkable Electrospun Nanofiber/Epoxy Nanocomposite Interlayers for Superior Laminated Composites**" and one journal article manuscript prepared for Composites Part B "**Nanofiber/ Epoxy Laminated Nanocomposites by Resin Film Infusion Molding**". The abstracts are provided in following section. The references are provided as a self-stand section at the end of the thesis.

Manuscript abstract for Composites Part B:

Nanofiber/Epoxy Laminated Nanocomposites by Resin Film Infusion Molding

Nanofibrous epoxy matrix laminated nanocomposite is introduced due to a novel methodology which is an adaptation of conventional dry-reinforcement/resin film infusion strategy. Electrospun polymeric nanofiber mats are embedded into epoxy and laminated by the process. Stacking of nanofiber layers, thickness, and shape of nanocomposites molded with the proposed technique could be customized conveniently according to the specific design of test method and associated sample. Commercial electrospun nanofibrous mats, are utilized in this study to demonstrate the concept. Stand free properties of the nanocomposite constituents (morphology, thermal properties, and tensile behavior), wettability, and nanocomposite cure cycle analysis are examined prior to inspection of flexural and tensile strength of nanocomposites. Cross-section of the nanofiber/epoxy laminated nanocomposite suggests promising laminated order of nanofiber mats and epoxy. Tensile strength and modulus of nanocomposites were modified by 25% and 9% respectively by integration of X nanofibers in 1.1wt%. Furthermore, incorporation of 3.7 wt% nanofibers altered flexural modulus of nanofiber/epoxy laminated nanocomposite with 35.6%. SEM fracture surface analysis of nanocomposites failed under tensile revealed their improved mechanical properties and ordered dispersion reinforcements.

Abstract of the currently under review journal article submitted to Composite Science and Technology:

Synergistic role of In-Situ Crosslinkable Electrospun Nanofiber/Epoxy Nanocomposite Interlayers for Superior Laminated Composites
Adopting a multi-scaled/hierarchical toughening approach, we have produced

nanofiber-reinforced epoxy laminate composites with superior toughness as a consequence of built-in, thermally catalyzed cross-linking between the nanofiber and the epoxy matrix, in addition to the usual curing within the epoxy itself. The nanofiber composition of P(St-co-GMA)/TBA-PA is designed such that the cross-linking agent PA groups are catalyzed by the thermally stimulated TBA initiators and inherent epoxy-nanofiber interfacial quality is promoted for toughening purposes. These nanofibers are electrospun onto two forms of the same base epoxy—neat resin films and pre-preg plies containing unidirectional carbon fibers. The nanofiber/epoxy nanocomposite specimens are manufactured via an in-house hot-press film molding method. DSC analyses reveal an increase in exothermic curing enthalpy, consistent with cross-linking between the epoxide groups of the fiber and epoxy matrix occurring in-situ, $i.e.$, triggered and advanced during the epoxy curing cycle. Analysis of the curing kinetics, following Ozawa-Flynn-Wall method, shows that the P(St-co-GMA)/TBA-PA nanofibers have a significant autocatalytic effect on the epoxy matrix curing. Increases in tensile strength (30%) and elastic modulus (8%) are measured over the un-reinforced epoxy cast specimens. Furthermore, end-notched flexure tests reveal a 95% increase in G_{IIC}, due to the incorporation of a single P(St-co-GMA)/TBA-PA nanofiber interlayer into laminated carbon fiber-reinforced composite of $(0)_{48}$ lay-up configuration. These results suggest that the self-initiated cross-linking between the nanofibers and surrounding epoxy matrix synergistically forms interlayer zones that contribute to toughening. Analysis of the fracture surface is presented to elaborate on the significant role of the proposed in-situ cross-linked nanofibers on the remarkable improvements in mechanical behavior of these laminated nanocomposites.

16

CHAPTER 2

 METHODOLOGY

2.1.Experimental methodology

One of the main contributions of the present thesis work is the introduction and demonstration of the nanocomposite fabrication method which is an adaptation of resin film infusion technique. The fabrication technique is expected to represent the in-situ formation of the nanocomposite interlayers when the nanofiber mats are laminated between the prepreg plies.

The step by step process of the manufacturing nanofiber/epoxy nanocomposites is schematically described in Figure 2. A layer of epoxy resin film is first laid on an aluminum caul-plate, then a self-supporting layer of electrospun nanofibrous mat is placed on the epoxy resin film (Figure 2B). The sequence of the layers, resin film and nanofibrous veil is multiplied until the desired configuration is achieved. For instance, tensile test specimen (UTM and DMA) configuration/lamination was by 2 layers of electrospun nanofiber mat and 3 layers of epoxy resin film (Figure 2C). A custom-made dog-bone shaped template of Teflon sheet (similar to Figure 2A) in accordance with ISO 527 is placed at the top layer of the stack and beneath the upper Aluminum plate in order to form tensile specimens. This eliminates the need for razor cut and cracks that might appear while cutting the sample (Figure 2E). Dimensions of the dog bone shaped nanocomposites were 150 mm× 20 mm × 0.6 mm. Another Teflon template (Figure 2A) was prepared, 20 mm×5mm×0.6mm in size, for dynamic mechanical analysis of the nanocomposite specimens in tensile mode. Reference neat epoxy tensile test specimens were processed by stacking 3 layers of epoxy resin film. As for the flexural strength of nanofiber reinforced laminated epoxy nanocomposites under three point bending test (UTM), the same specimen molding procedure was followed, but in accordance with ASTM D 790 – 02 to obtain samples of size 100 mm× 14.5 × 1.4mm. These bending specimens were manufactured by laminating 20 layers of electrospun nanofiber mats and 21 layers of epoxy resin film. Reference neat

epoxy specimens were manufactured by stacking 21 layers of epoxy resin film. In all geometries, once the stacking is done (Figure 2, C) the open area between to aluminum caul-plates has been sealed to avoid the excessive flow of the resin during the cure cycle. Then, nanocomposite lay-up was vacuum bagged, placed into heating press and heated at a rate of 1°C/min up to 140°C. The nanocomposite was kept at 140°C for 1 hour while uniform pressure of 2 bars was maintained (Figure 2D). Fiber weight fraction of the processed nanofiber/epoxy laminated nanocomposites is reported in Table 2. As depicted in Figure 2E. processed nanocomposites could be removed easily from the Teflon template in pre-designed geometry and with highly smooth surface on both sides of the samples. Figure 3A represents fiber-matrix interface region in the cross section of X / epoxy laminated nanocomposites depicted in Figure 3B.
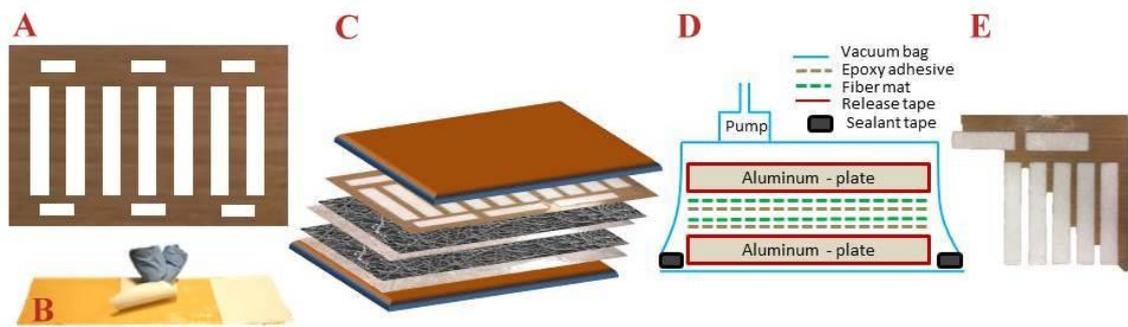
Figure 2 A schematic descriptions for the manufacturing of electrospun nanofiber/epoxy laminated nanocomposite by resin film molding. A: Custom-made Teflon template; B: Snap-shot from hand lay-up of self-supporting electrospun nanofiber mats on an epoxy film; C: Sample set of nanofiber/epoxy laminated nanocomposite with 2 layers of electrospun nanofiber mat, 3 layers of epoxy film, and Teflon template place on the most top ply molded between aluminum plates; D: Vacuum bagging configuration; E: laminated nanocomposite test specimens from custom made Teflon template after manufacturing without need for razor cut.

Table 2 Average nanofiber weight percent in nanofiber/epoxy laminated nanocomposites. T: Tensile, B: Bending

Nanocomposite system	Resin film layers	Nanofibrous veil layers	Nanofiber wt%	Standard/test mode
PA6/epoxy	3	2	1	ISO 527/ T
PAN/epoxy	3	2	1	ISO 527/ T
PVB/epoxy	3	2	1	ISO 527/ T
X/epoxy	3	2	1	ISO 527/ T
X/epoxy	21	20	3.7	ASTMD790–02/B

2.2. Materials

As the proposed fabrication technique is applicable literally for any nanofiber types, different choices of base polymer or nanofiber can be studied. Having said that, several nanofibers were incorporated and compared. To eliminate disadvantages of nanofibers spun by needle based spinneret commercially available nanofibrous mats of Xantulayer (labeled herein as X) processed by Revolutionary Fibers Ltd [17] with sonic needleless electrospinning technology [5] and veils of PA6, PAN, and PVB with needleless force spinning technology processed by FiberRio, Elmarco [5] were supplied from Pardam nanotechnology [62]. Aerial weights of nanofibrous veils are reported in Table 3. Epoxy resin film with aerial weight of 113.4 g/m^2 was purchased from c-m-p gmbh company [63].

Table 3 Aerial weights and electrospinning techniques of the nanofibrous veils.

Nanofiber Mat	Aerial wt (g/m^2)	Company name	electrospinning technique Patent	Machine
Xantulayer (X)	3	Revolutionary Fibers Ltd	Sonic Needleless	Own design/ Trade secret
PA6	3.4	Pardam nanotechnology	ForceSpinnig, Needleless	FibreRio, Elmarco
PAN	3.2	Pardam nanotechnology	ForceSpinnig, Needleless	FibreRio, Elmarco
PVB	3.1	Pardam nanotechnology	ForceSpinnig, Needleless	FibreRio, Elmarco
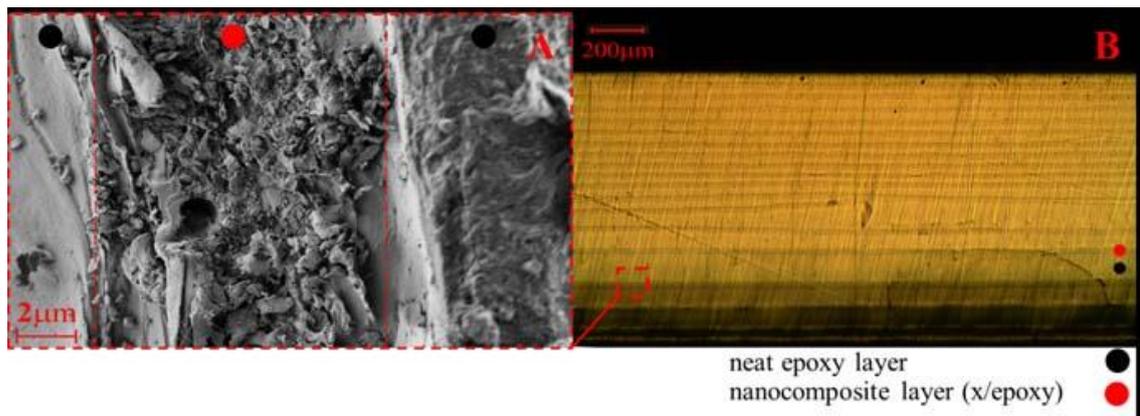
Figure 3 Cross-section of the nanofiber reinforced laminated epoxy nanocomposite. (B) Optic microscope image of the nanofiber reinforced epoxy nanocomposite. Scale bar: 200 μm (A) SEM image of the fiber-matrix interface in the nanocomposite. Scale bar: 2μm. Epoxy matrix is indicated by black circles and nanocomposites (epoxy infused nanofiber veils) by red circles.

2.3. Mechanical Tests

Testing for mechanical behavior of the nanocomposites under tensile and flexural loading was carried out by using Zwick/ Roell, Z100 Proline universal testing machine (UTM). Stiffness and strength of the laminated nanocomposites were studied using the dog-bone type tension specimens in accordance with ASTM D 638-03. Dimensions of the neat epoxy and nanocomposite specimens were 25 mm in width, 100 mm in length, and average thickness of 0.6 mm. For precise stiffness measurement, extensometer was installed and gauge length was set to 25 mm. Flexural strength of nanocomposites were determined according to ASTM D 790-02, for which the specimen dimensions were 15 mm in width, 100 mm in length and 1.4 mm thick. Tensile and three point bending tests were conducted at room temperature 25°C with a machine crosshead displacement rate of 2 mm/min. To extract average stand free mechanical properties of X, PA6, PAN, and PVB electrospun nanofiber mats as also reported in literature, e.g. [64–66], tensile specimens with 3 cm in width and 9 cm in length were cut and paper pads of 3cm× 3cm (same size as the testing grips) were glued to the both ends of the mat samples. Tensile tests of the mats were conducted at room temperature 25°C using a 200 N load-cell, loading at a displacement rate of 1 mm/min. On each test mode, five specimens of their own kind of the neat epoxy, nanocomposite and fiber mat were tested.

2.4. Dynamic Mechanical Analysis (DMA)

Dynamic mechanical analysis is included in order to assess fiber-matrix interface-related properties of the nanocomposite [27,60,67–69]. Our samples prepared for DMA were tested on a Netzsch − DMA 242 C from 25℃ to 160 ℃ at a dynamic temperature scanning rate of 2 °C/min. The tests were operated in the tension mode at an oscillation frequency of 1 Hz. Dynamic strain sweep was first performed to determine linear viscoelastic range of the samples. Amplitude was set on 10 μm with a proportional factor of 1.1 and dynamic force of 7N. Tensile DMA samples of neat epoxy (3 layers of epoxy film) also X, PA6, PAN, and PVB electrospun nanofibrous mat reinforced

laminated epoxy nanocomposites (2 veils/ 3 epoxy film layers) were prepared with 20 mm in length, 5 mm in width, and 0.6 mm thick. Three samples from each type of laminated nanocomposite were tested. The storage modulus (E') and the loss tangent (tanδ) were measured and reported for each sample type.

2.5. Microscopic Characterizations

The morphology of the X, PA6, PAN, and PVB nanofiber mats, fiber diameter distribution and fracture surfaces of the specimens, were examined by using LEO 1530VP scanning electron microscope (SEM). It was operated employing secondary electron detector and in-lens detector at 2–5 kV after carbon coating of the specimens. In addition, cross-sectional inspection of the laminated epoxy nanocomposites were done under Nikon Eclipse ME 600 optical microscope in order to assess the uniformity and sequential distribution of reinforcing layers of electrospun nanofibrous mats. Furthermore, wettability of X, PA6, PAN, and PVB nanofiber mats was assessed by contact angle measurements performed using the Attension Theta contact angle measurement system which is equipped with an optical microscope. Liquid epoxy (Hunstman.Adv.Mat.Co.Araldite.LY 564 and XB 3404), was utilized as the wetting liquid for the contact angle measurements.

2.6. Thermal Analyses by Differential Scanning Calorimetry (DSC)

Thermal characteristics of neat epoxy, X/epoxy, PA6/epoxy, PAN/epoxy, and PVB/epoxy nanocomposites were inspected with Q2000 (TA instruments) Differential Scanning Calorimetry (DSC). To monitor morphological transformations in electrospun nanofibrous mats of X, PA6, PAN, and PVB they were probed on dynamic heating mode ramped in 5℃ /min from 25℃ until 250℃. To assess total reaction enthalpy (ΔH_t) of the neat epoxy, X/epoxy, PA6/epoxy, PAN/epoxy, and PVB/epoxy nanocomposites (one layer from each), associated samples were cured in DSC on dynamic heating mode

scanned with a heating rate of 5 ℃/min from 25℃ until 200℃. Then, samples were cooled down until 25℃ with a rate of 10℃ /min to detect possible recrystallization peaks. In order to examine in-situ curing of the nanocomposites, samples of the neat epoxy film, PA6/ epoxy, PAN/ epoxy, and PVB/ epoxy were cured in DSC on isothermal mode at 140℃ for 1 hour ramped from 25℃ with a heating rate of 5 ℃ /min.

CHAPTER 3

AN ASSESSMENT ON VARIOUS POLYMERIC NANOFIBERS AS NANOCOMPOSITE REINFORCEMENT

3.1. Overview

Nanofibrous epoxy matrix laminated nanocomposite is introduced due to a novel methodology which is an adaptation of conventional dry-reinforcement/resin film infusion strategy. Electrospun polymeric nanofiber mats with different base polymers were embedded into epoxy and laminated by the process. Stacking of nanofiber layers, thickness, and shape of nanocomposites molded with the proposed technique could be customized conveniently according to the specific design of test method and associated sample. Commercial electrospun nanofibrous mats of Xantulayer, PA6, PAN, and PVB were utilized in this study to demonstrate the concept. Stand free properties of the reinforcement choices as nanocomposite constituents (morphology, thermal properties, and tensile behavior), wettability, and nanocomposite cure cycle analysis were first examined and graded prior to inspection of tensile strength of nanocomposites. Tensile strength of nanocomposites were modified in some cases (e.g. X/epoxy) up to 25% by integration nanofibers in 1.1wt%. SEM fracture surface analysis of nanocomposites failed under tensile revealed their improved mechanical properties and ordered dispersion reinforcements.

3.2. Stand free Constituent Properties

3.2.1. Morphology of X, PA6, PAN, and PVB Nanofibrous Mats (by SEM and DSC)

Electrospun nanofiber mats as reinforcing agents in X/epoxy, PA6/epoxy, PAN/epoxy, and PVB/epoxy laminated nanocomposites should be manufactured at the processing temperature below their melting temperature (T_m) to preserve their non-woven fibrous network structure [70] and bear the applied loads efficiently. Figure 4 reports thermal

behavior of X, PA6, PAN, and PVB nanofiber mats scanned with Differential Scanning Calorimetry (DSC). The processing temperature of nanocomposites 140℃ is marked by dashed line. Complementary to DSC results, Figure 5 gives insight into the thermal properties of nanofibrous veils with SEM images of X, PAN, PA6 and PVB in the pristine condition (Figure 5A, C, E, G) and as heat treated (Figure 5B, D, F, H) on a hot plate following identical cure cycle of nanocomposite processing procedure, which is a ramp from room temperature to 140 °C at a heating rate of 2°C /min. Assessment of SEM and DSC results are reported as follows:

X is thermoplastic polyamide (PA66) [19] based electrospun nanofiber veils developed by Revolutionary Fibers Ltd marketed as Xantulayer (herein labeled as X) as, to our knowledge, the world's first commercially available nanofiber interleaving veil known for improved interlaminar fracture toughness (ILFT), compression after impact strength (CAI), and fatigue resistance of composite laminates [5]. In DSC analysis of X nanofiber mat in Figure 4 no endothermic reaction (i.e. melting) was detected until the processing temperature of nanocomposites 140°C. Its melting point was found at 265°C. Morphological analysis of X nanofiber mat at 25°C (average diameter 309nm) and 140°C (average diameter 214nm) reported in Figure 5A and B also proves their nonwoven morphology to be conserved at the processing temperature of nanocomposites. As a result, potential of X nanofibers to be employed as reinforcement in manufacturing nanofiber/epoxy laminated nanocomposite was confirmed.

PVB nanofibers are reported in the literature as an amorphous [71] nanofibers with thermoplastic characteristics [72] characteristics known for high toughness, good adhesive properties [35,73]. The glass transition temperature of PVB nanofibers in Figure 4 was detected at 73℃ as in the literature e.g. [74]. No melting transition was noticed for PVB nanofibers. An exothermic reaction between150℃-300℃ with peak temperature at 296℃ was ascribed to decomposition of PVB nanofibers. Morphology of PVB electrospun nanofiber mats as it is and after exposure to 140℃ is reported in Figure 5G and Figure 5H respectively. It is observed that nonwoven structure of PVB

nanofiber mat at pristine condition with average nanofiber diameter of 1166 nm has lost in at140℃.

PA6 nanofibers are known as thermoplastic with crystalline structure with two crystalline forms namely α and γ [75,76] as in Figure 4 with high-temperature endothermic peak observed at 222 ± 3 ℃ ascribed to the α form and the detected low-temperature endothermic peak at 186± 3 ℃ corresponds to the γ form [76]. These endothermic peaks are attributed to an enthalpic relaxation process of an interphase between the crystalline and amorphous phases [77]. Nonwoven morphology of PA6 nanofiber mat at 25℃ in Figure 5C is preserved at the nanocomposite processing temperature 140℃ Figure 5D. Average PA6 nanofiber diameter at 25℃ equal to 354 nm decreased to 324.7 nm at 140℃.

PAN is nanofibers are known as thermoplastic polymer with semi-crystalline structure. In Figure 4 a weak glass transition tempearture exhibited at 117℃, were followed by a sharp exothermic peak at 286℃. This sharp exothermic peak could be ascribed to the nucleophilic attack at a nitrile followed by instantaneous cyclization reaction to an extended conjugated structure [78]. No endothermic peak (e.g. melting peak) were detected for PAN nanofibers in Figure 4. Nonwoven morphology of PAN nanofibers at 25℃ shown in Figure 5E is generally conserved at 140℃ as only amorphous fraction of PAN nanofibers softened according to Figure 5F. The as is average diameter of 768 nm is reduced at 140℃ to 741.3 nm as depicted in Figure 5F.
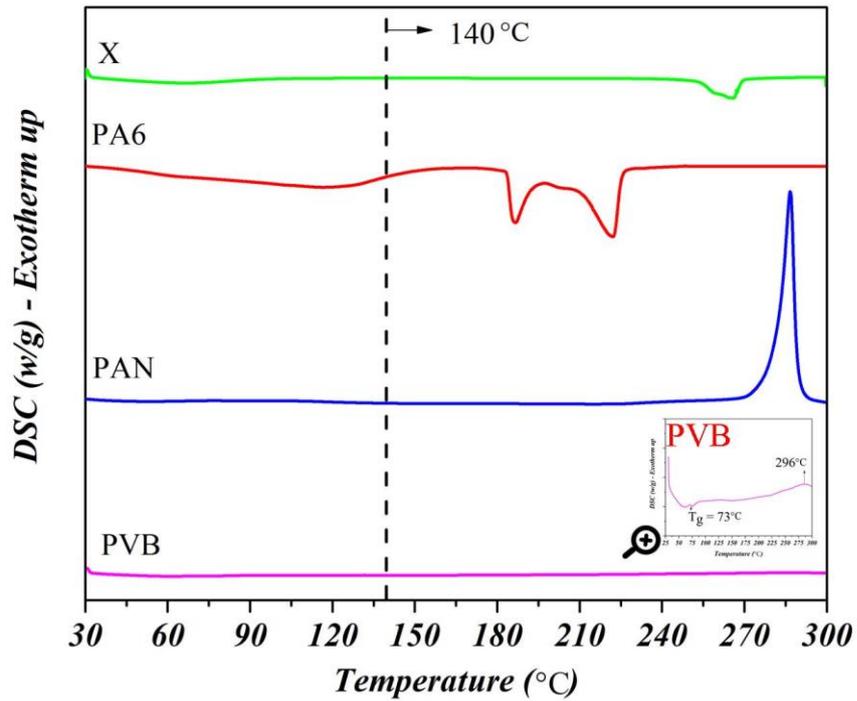
Figure 4 DSC Heating cycle of X, PAN, PA6, and PVB electrospun nanofiber mats scanned from 25℃ up to 250°C with a heating rate of 5°C/min. To check nanofibers ability to hold their integrity at the processing temperature, the curing temperature of the nanofiber/epoxy laminated nanocomposites 140°C is demonstrated with dashed line. Exotherm: Up.
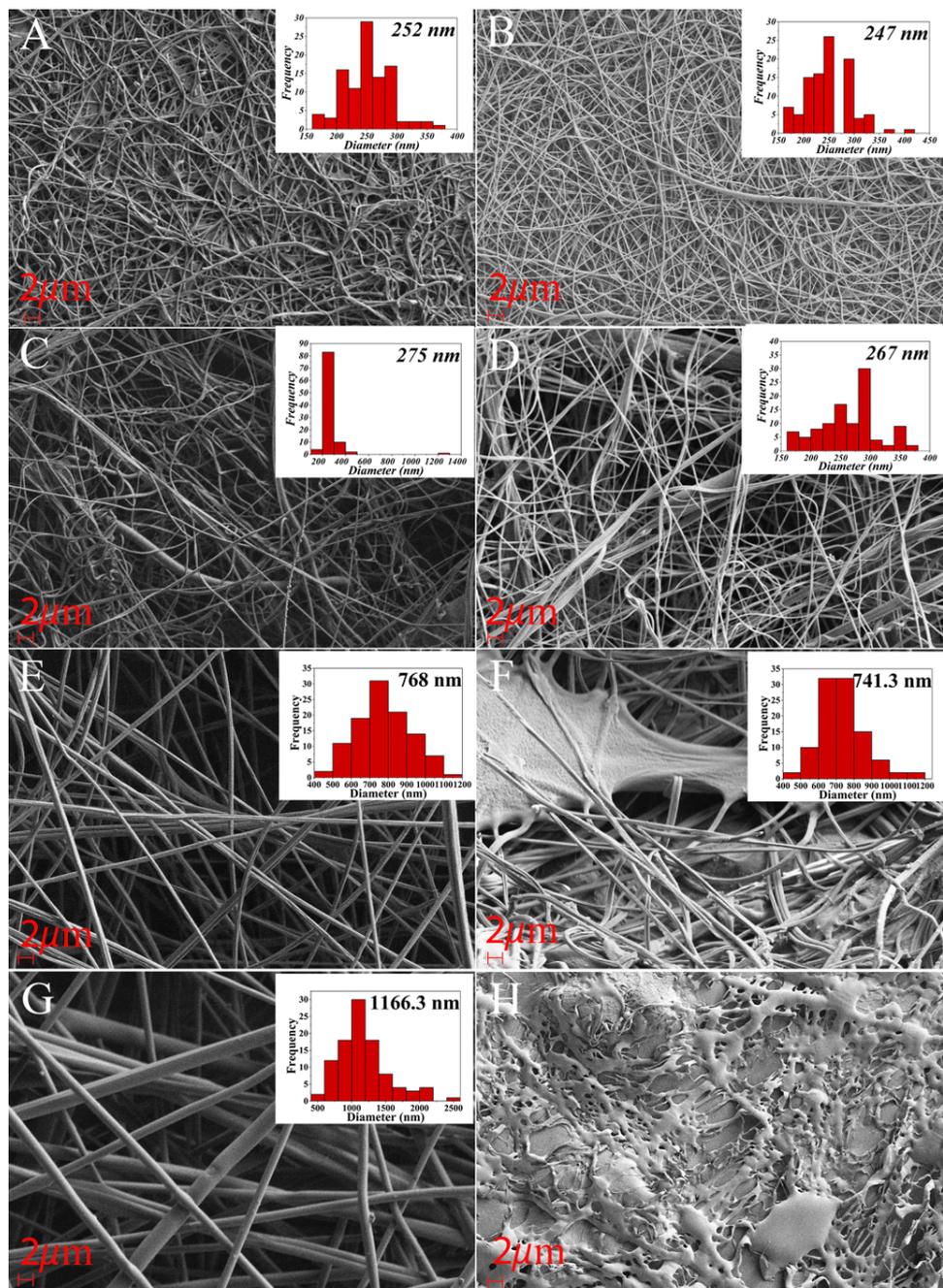
Figure 5 SEM images of electrospun nanofiber mats in pristine condition and after heat treated in hot plate at 140℃. (A) X nanofiber mat at 25℃. AD: 308 nm (B) X nanofiber mat at140℃. AD: 214 nm. (C) PA6 nanofiber mat at 25℃. AD: 355.7nm (D) PA6 nanofiber mat at 140℃. AD: 324.17nm (E) PAN nanofiber mat at 25℃. AD: 768nm. (F) PAN nanofiber mat at 140℃. AD: 741nm (G) PVB nanofiber mat at 25℃. AD: 1166.3 nm (H) PVB nanofiber mat at 140℃. Scale bars: 2μm

3.2.2. Tensile Behavior of Electrospun Nanofibrous Mats

Tensile testing of the X, PA6, PAN, and PVB electrospun nanofiber mats are reported in Figure 6. Five samples of each electrospun nanofiber mat with nearly same areal weight were tested. Stress-strain curves of stand free nanofiber mats suggest an initial elastic region followed by a plastic-like deformation region. Elastic modulus of X determined as 185.8 ± 13 MPa as the extreme case was 428% higher than elastic modulus of PVB 35 MPa. Ultimate tensile strength, elastic modulus, and average aerial weight of X, PA6, PAN, and PVB veils are reported in Table 4. The large strain before failure in nanofibers attributed to the polymeric nature of nanofibers and the presence of overlapped non-woven, randomly oriented layers that can progressively be aligned in the loading direction. A fractured view of a nanofiber mat tensile specimen is provided in Figure 6 (B). Consistency of the stiffness for a given nanofiber choice was considered reasonable whereas variation of the strain at failure should be noted.

Nanofiber Fracture
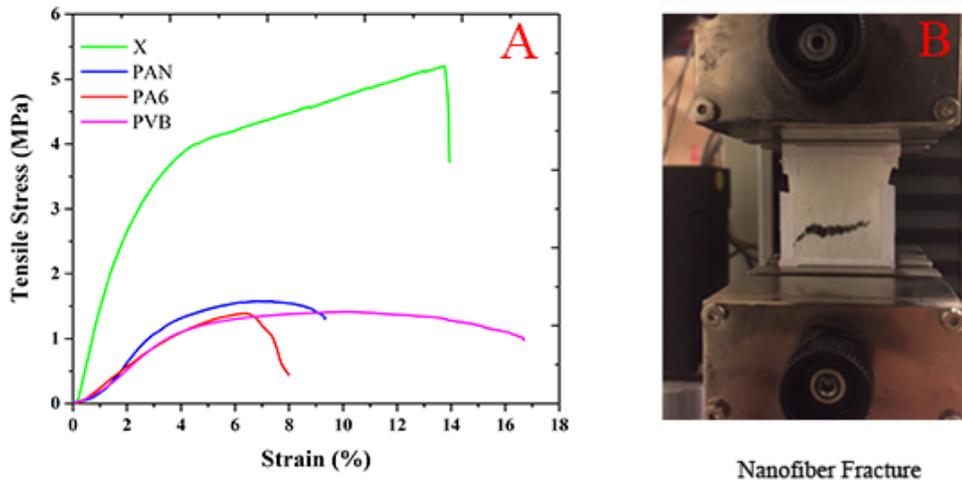
Figure 6 A: Tensile behavior of the X, PA6, PAN, and PVB electrospun nanofiber mats conducted in UTM. B: Representative fracture mode of electrospun nanofiber mats tested under tensile load with UTM.

Table 4 Aerial weight, elastic modulus, and tensile strength of X, PAN, PA6, and PVB veils.

Electrospun nanofiber mat	Aerial weight (g/m^2)	Elastic Modulus (MPa)	Strength (MPa)
X	3	185.8 ± 13	8.39 ± 0.75
PA6	3.4	31.3 ± 2.5	1.34 ± 0.1
PAN	3.2	84 ± 4.5	1.67 ± 0.2
PVB	3.1	35 ± 2.9	1.46 ± 0.1

3.2.3. Tensile Behavior of Neat Epoxy

Mechanical test results of the neat epoxy samples were used as reference in assessment of the tensile behavior of X, PA6, PAN, and PVB nanofiber/epoxy laminated nanocomposites. Tension test stress-strain curves and pictures of the specimens after failure are provided in Figure 7A and B respectively. The recorded reference average properties due to five samples are: elastic modulus: 2758 ± 58 MPa, ultimate tensile strength: 48 ± 5 MPa, and percent elongation at failure: $\%2 \pm 0.36$. Brittle fracture of the neat epoxy samples can be noted from the stress-strain curves with minor nonlinearity and fracture modes are depicted in Figure 7 (B).
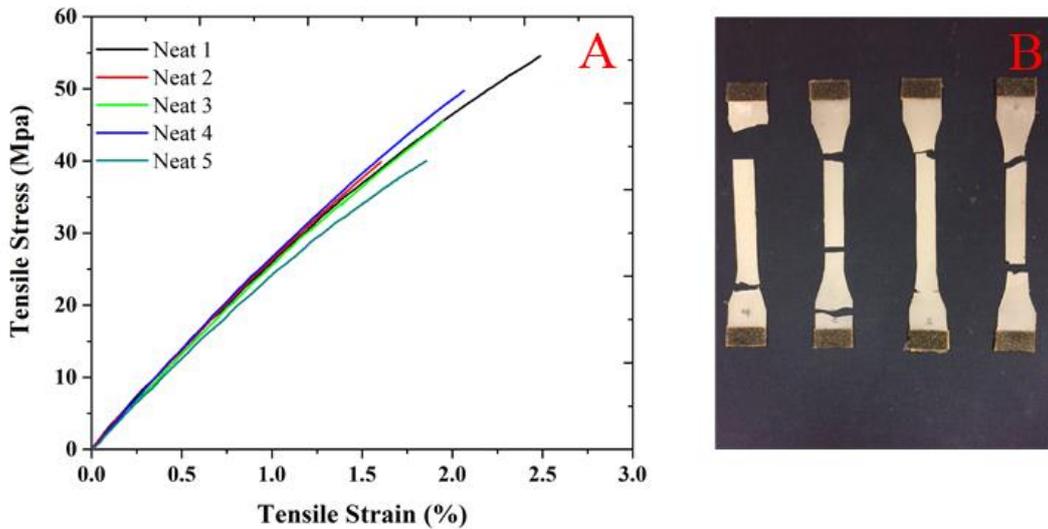
Figure 7 A: Tensile behavior of the neat epoxy dog-bones test with UTM. B: Images of the Neat epoxy samples failed under tensile load with UTM.

3.3. Characterization for Nanocomposite Processability

3.3.1. Wet-ability of fiber mat reinforcing layers by epoxy

Quality of interfacial adhesion and compatibility between the nanocomposite constituents is crucial for effective fiber-matrix load transfer and composite performance. To assess fiber-matrix compatibility and interfacial characteristics, wettability of X, PA6, PAN, and PVB nanofibers was inspected by contact angle measurements. Furthermore the standing-free mat/epoxy film stacks of X, PA6, PAN, and PVB were exposed to curing temperature of the epoxy film 140°C (without applying any pressure) and SEM image of the stacks followed by the heat treatment are reported to provide more insight. As depicted in Figure 8 (A) epoxy droplet (Hunstman.Adv.Mat.Co.Araldite.LY 564 and XB 3404), deposited on the X nanofiber mat fully impregnated the X nanofiber mat in about 180 seconds. This is attributed to positive attractive cohesive forces between X nanofiber mat and epoxy resin that can compensate for negative capillary pressure [40,51,79]. Figure 8B represents the SEM

31

image of the stack followed by the heat treatment. It shows that the epoxy film completely wetted the X nanofiber mat upon its conversion into intermediate liquid phase. This demonstration was considered as the preliminary evidence for the nanofiber-matrix adhesion, and potential for successful mechanical performance of anticipated nanofiber/epoxy film nanocomposite. Further results of contact angle measurement and SEM images of standing free mat/epoxy stacks of PA6, PAN, and PVB nanofiber mats exposed to 140°C without applied pressure are reported in Figure 8A. Impregnation of epoxy droplet deposited on PA6 (Figure 8C) and PAN (Figure 8E) in 17 seconds and 23 seconds respectively accrued in shorter time span with respect to X. This might be attributed to the large pore size in PA6 and PAN nanofibrous veils.

Table 5 Summary of the wettability analysis for X, PA6, PAN, and PVB nanofibrous veils

Nanofiber mat	ECA	standing free mat/epoxy morphology
X	Smooth/ 180 seconds	Excellent fiber-matrix interface/ nonwoven morphology preserved
PA6	Smooth/17 seconds	good fiber-matrix interface/ nonwoven morphology preserved
PAN	Wetting is not continuous / 23 seconds	fair fiber-matrix interface/ nonwoven morphology preserved
PVB	Smooth/ 180 seconds	Nonwoven morphology has lost due to nanofiber melt

ECA: Epoxy drop Contact Angle
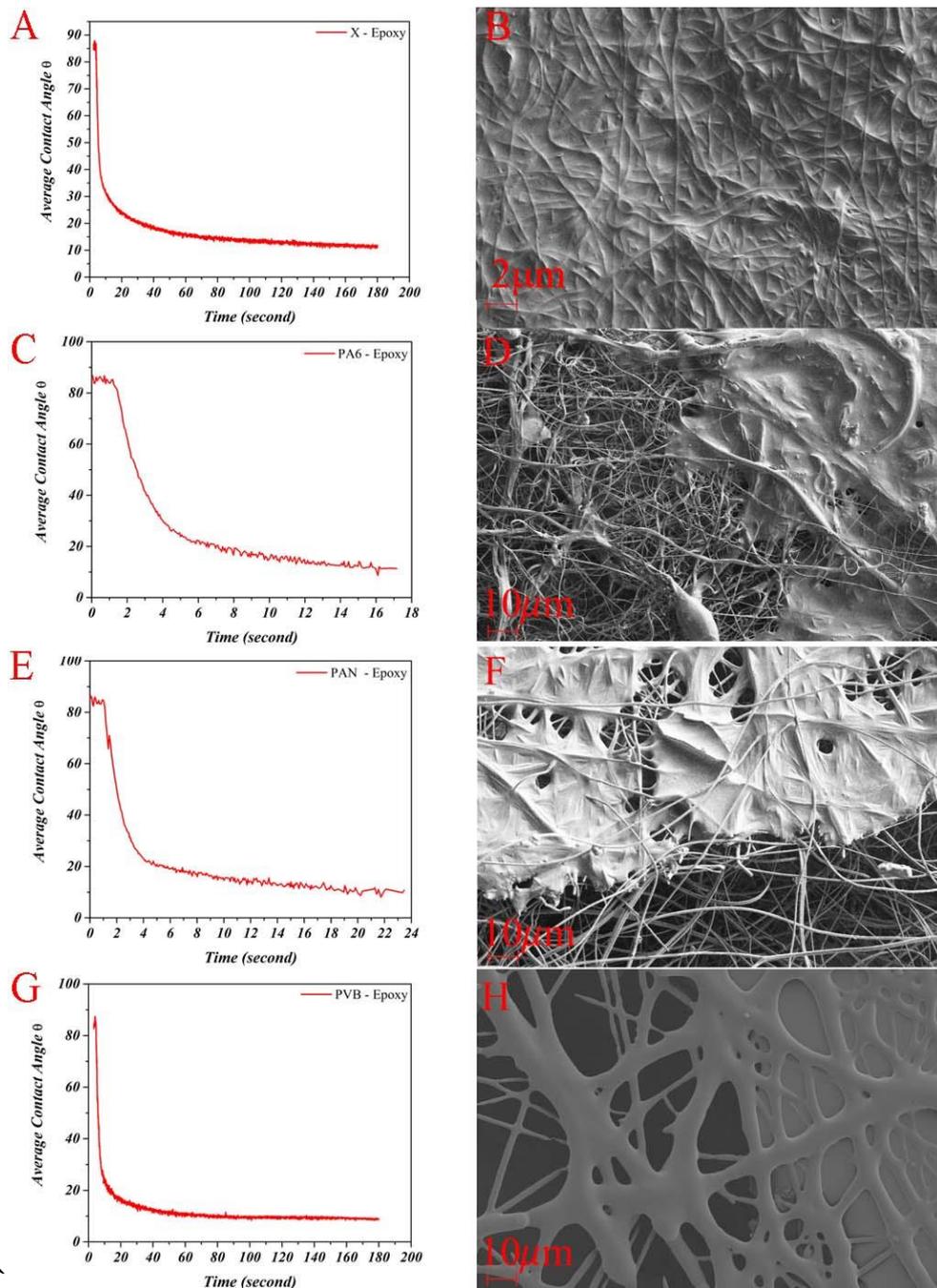
Figure 8   Fiber-matrix interfacial adhesion analysis (A, C, E ,G) Contact angle measurment of water and epoxy droplet on X, PA6, PAN, and PVB electrospun nanofibrous mat at 25°C (B, D, F, H) SEM images of free-standing fiber-matrix self-adhesion at the processing temperature of 140°C. Scale bar: 2μm

3.3.2. Thermal Behavior of Nanofiber/Epoxy Nanocomposites

Neat epoxy film, X, PA6, PAN, and PVB nanofiber/epoxy samples were studied by Differential Scanning Calorimetry (DSC) on dynamic heating mode scanned from the room temperature 25°C up to 225°C. Figure 9 (A) reports the thermal behavior in dynamic mode. Total curing enthalpy (ΔH_{total}) of the neat epoxy is equal to 350 J/g whereas X/epoxy has cure enthalpy of 285 J/g which is 18.6% lower than that of neat epoxy. As reported in Table 6 total cure enthalpy of PA6/epoxy, PAN/epoxy, and PVB/epoxy are 47%, 12.3%, and 16% lower than the neat epoxy. Peak temperature of the neat epoxy curve in Figure 9A (140°C) was selected as the processing/cure temperature for the nanocomposites. It is below melting temperature (T_m) of the nanofiber mats determined by the thermal analyses of the nanofibers. Furthermore, Figure 9 (B) provides isothermal curing enthalpy (ΔH_{iso}) of the X/epoxy, PA6/epoxy, PAN/epoxy and PVB/epoxy as reported in Table 6 which is to simulate curing at 140°C for 1 hour. Furthermore, degree of cure (α) defined by $\Delta H_{iso}/\Delta H_{total}$ as a measure of degree of cure for nanocomposites at the processing temperature 140°C are provided in Table 6 [80,81]. Degree of cure for neat epoxy, X/epoxy, PA6/epoxy, PAN/epoxy, and PVB/epoxy cured at 140°C is equal to 0.9, 0.96, 0.92, 0.68, and 0.9.

34
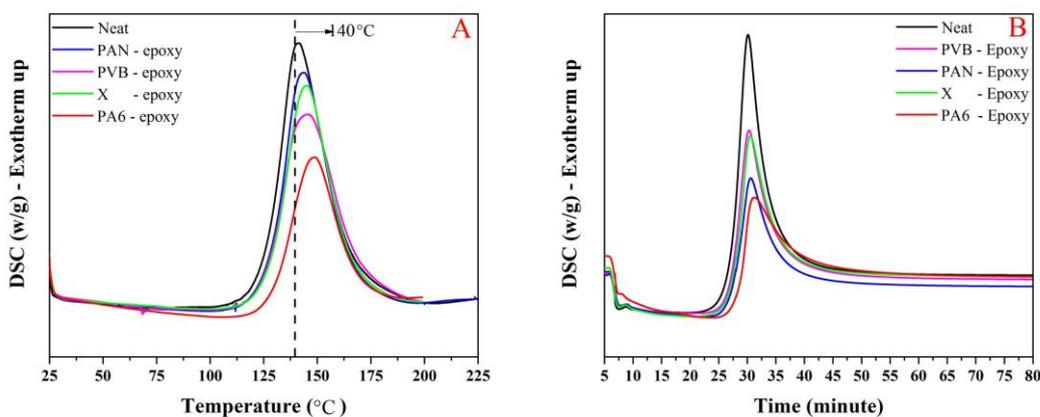
Figure 9 Cure cycle analysis of neat epoxy, X/epoxy, PAN/epoxy, PA6/epoxy, and PVB/epoxy performed by DSC. A: full curing cycle of neat epoxy, X/epoxy, PA6/epoxy, PAN/epoxy, and PVB/epoxy scanned on dynamic mode from 25°C until 200°C. B: Isothermal cure cycle of neat epoxy, X/epoxy, PA6/epoxy, PAN/epoxy, and PVB/epoxy ramped by 5°C/min rate from the room temperature 25°C up to the curing cycle of nanocomposites 140°C and cured for 1 hour.

Table 6 Summary of the thermal properties of neat epoxy, X/epoxy, PA6/epoxy, PAN/epoxy, and PVB epoxy conducted by DSC

Nanocomposite	ΔH_{total} (J/g)	ΔH_t (J/g)	α (%)
Neat Epoxy	350	315	0.9
X/Epoxy	285	274	0.96
PA6/Epoxy	185	171	0.92
PAN/Epoxy	307	208	0.68
PVB/Epoxy	295	267	0.9

3.4. Mechanical behavior of fiber reinforced laminated nanocomposites

3.4.1. Tensile Testing Results for nanocomposite specimens (UTM)

Higher strength and elongation at failure compared to neat epoxy was anticipated in X, PA6, PAN, and PVB nanofiber/epoxy laminated nanocomposites. Figure 10 represents tensile behavior of the neat epoxy specimen (with three layers of epoxy resin film) and nanofiber reinforced laminated epoxy nanocomposites (with 2 layers of X nanofiber mat and 3 layers of epoxy resin film). Results in Table 7 suggest that two layers of X electrospun nanofiber mat elevated the stiffness of the laminated neat epoxy nanocomposites 3000$\pm$ 250 MPa, about 9% increase compared to the neat epoxy stifness 2758$\pm$ 58 MPa. Furthermore, the ultimate tensile strength of the X nanofiber reinforced laminated epoxy nanocomposites is superior, increased by about 25 % with respect to the neat sample. Incorporation of 1.1 wt% PAN and PA6 nanofibers modified the stiffness of the neat epoxy by 10.3% and 1.5%. Although the ultimate tensile strength and percent elongation at failure of PA6/epoxy nanocomposites are superior that neat epoxy by 19%, the ultimate tensile strength and percent elongation at failure of neat epoxy were deteriorated by 25% and 27% respectively by incorporation of PAN nanofibers. Furthermore, 1.1 wt% of PVB nanofibers increased the nonlinearity in the tensile behavior of the neat epoxy and increased the elongation at failure by 10%. However, both the ultimate tensile strength and the elastic modulus of the neat epoxy were negatively affected by 6%.
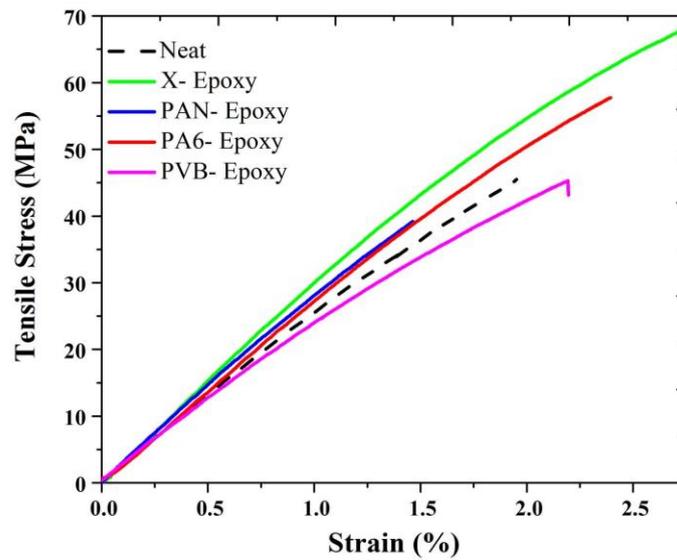
Figure 10 Tensile testing of the neat epoxy (made by 3 layers of epoxy film), X, PA6, PAN, and PVB nanofiber mat reinforced laminated epoxy nanocomposite (made by 2 layers of X nanofiber mat and 3 layers of epoxy film)

Table 7 Tensile properties of neat epoxy and X/epoxy, PA6/epoxy, PAN/epoxy, and PVB/epoxy laminated nanocomposites

Nanocomposite	# of epoxy layers	# of reinforcing layers	Fiber wt (%)	Stiffness (MPa)	Failure strength (MPa)	Elongation at failure (%)
Neat epoxy	3	0	0	2658± 58	48± 5	2±0.3
X/epoxy	3	2	1.1	3000± 250	60.3± 4	2.42±0.2
PVB/epoxy	3	2	1.1	2500±240	45±6	2.19± 0.8
PA6/epoxy	3	2	1.1	2700±400	57±6	2.39± 0.1
PAN/epoxy	3	2	1.1	2932±28	36±8	1.46± 0.4

3.4.2. Fracture Surface Analysis of Nanofiber/Epoxy Laminated Nanocomposites (SEM)

Fracture surface SEM images of the neat epoxy and X, PVB, PAN, and PA6 nanofiber/epoxy laminated nanocomposite (e.g. epoxy/X/epoxy/X/epoxy) tensile test specimens are provided in Figure 11, Figure 12, Figure 13, Figure 14, and Figure 15 respectively. In Figure 11 river line patterns, the typical attribute of the brittle fracture [82], are noticeable on the fracture surface of the neat epoxy. River lines map the direction of progressive crack front [82]. Bowed out fine river line patterns show local direction of crack growth such as those labeled with (F) in the direction of the arrow. Progressive increase in roughness of the fracture surface roots in high rate of energy released at the tip of the moving crack. The height and spacing of the river lines increase with crack length. At river line steps, overlapping cracks form lances such as L_1, L_2, and L_3 [82].Coalescence of river lines expanding on three levels (A, B, and C) with arrows indicating direction of river patterns is created a concave fracture surface. The resulted crack is propagated in direction (D). Ultimate failure of the specimen is prescribed to progress of crack front developed from smooth mirror region to lances, and overlapping cracks (D) moving towards sample edges. On the other hand, fracture surface of X /epoxy laminated nanocomposite with 2 layers of X electrospun nanofiber mat is shown in Figure 12. Nanocomposite fibrous zone in Figure 12A is sandwiched between brittle epoxy rich parts with evident lances (on the right edge of the sample) and river patterns. Higher fracture surface roughness of the epoxy regions in Figure 12 with respect to neat epoxy fracture surface in Figure 11 is pointing higher fracture toughness in X/epoxy laminated nanocomposite. Fracture surface morphology of nanocomposite zone is analyzed in Figure 12B to interpret higher tensile strength and stiffness of X-nanofiber/epoxy laminated nanocomposite according to Table 7. Morphology of the nanocomposite region suggests ductile nature of fracture surface without river patterns. Several nanofiber lateral (fibers in the plane of fracture) debonding marks spread over the nanocomposite fracture surface and fiber exposed at the bottom of Figure 12B are ascribed to high released energy upon failure which can

38

justify the enhanced mechanical properties of X/epoxy laminated nanocomposite in Table 7. Figure 13 depicts fracture surface of PVB /epoxy laminated nanocomposite. Although river lines are still detectable at the fracture surface of the PVB/epoxy nanocomposite the general fracture flow resemble lava and the fracture surface is similar to ductile fracture. The stress-strain curve of the PVB/epoxy laminated nanocomposite in Figure 10 indicates that PVB nanofibers have plasticizing effect on the epoxy matrix which could be traced in the ductile fracture surface topology of PVB/epoxy nanocomposite in the Figure 13. The fracture surface of PVB/epoxy nanocomposite did not reveal fibers and any sign of nanofiber debonding or nanofiber fracture which could be ascribed to the loss of fibrous structure at the nanocomposite processing temperature 140°C and leading to lower mechanical properties with respect to the neat epoxy. Fracture surface of the PAN/epoxy laminated nanocomposite is shown in Figure 14(A and B). It is highly rough with marking of progressive crack propagation. The I and II arrows represent river line patterns at the outer parts of the fracture surface which corresponds to the epoxy rich parts of the sandwich-like nanocomposite. Figure 14B represents fracture surface of the PAN/epoxy laminated nanocomposite at higher magnification with distinguished marks of lateral (fibers in the fracture plane) nanofiber debonding, nanofiber fracture, and exposed fiber which indicate high amount of energy released upon the sample fracture under tensile load. Furthermore, highly rough fracture surface of the PA6/epoxy laminated nanocomposite depicted in Figure 15 is in agreement with its high tensile characteristics demonstrated in Figure 10.
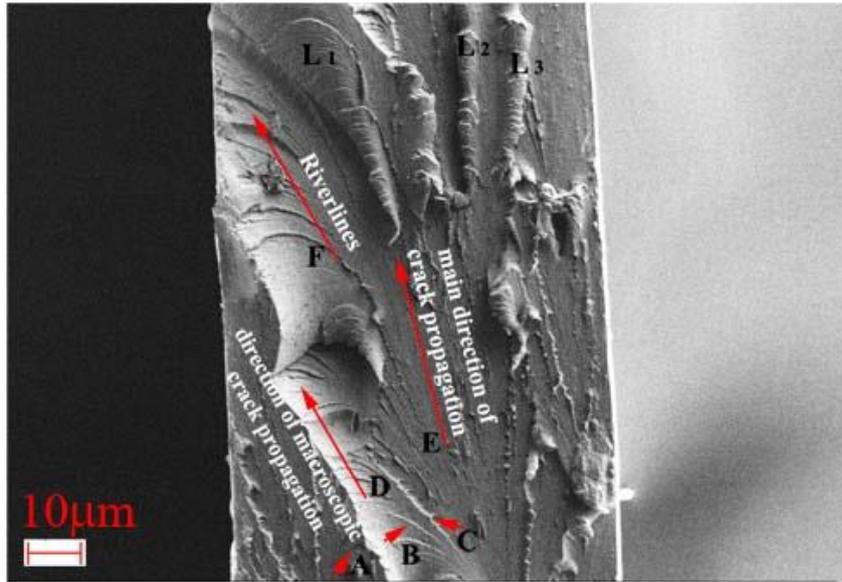
Figure 11 SEM image of neat epoxy fracture surface, failed in tensile test. Magnification: 1K; Scale bar: 10μm
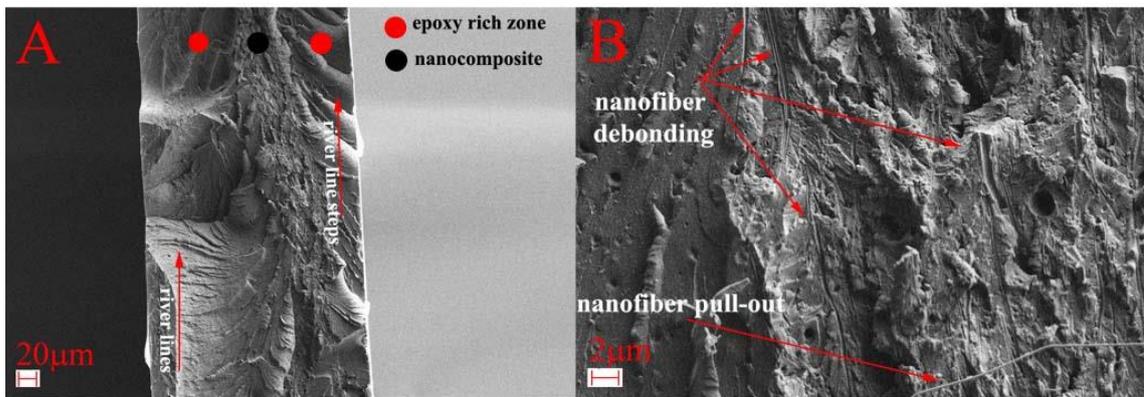
Figure 12 SEM image of X /epoxy laminatd nanocomposite fracture surface, failed in tensile test. (A) X nanofiber/epoxy laminated nanocomposite; Magnification: 500×; Scale bar: 20μm. (B) Magnified nanocomposite-epoxy interface region of the fracture surface. Magnification: 7.5K×; Scale bar: 2μm.
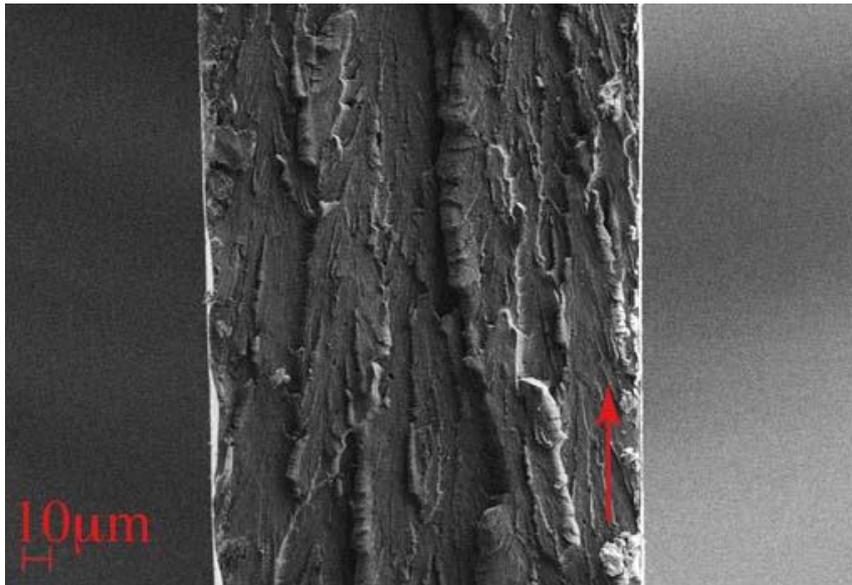
Figure 13 SEM image of PVB/ epoxy laminated nanocomposite fracture surface, failed under tensile load. Arrow:direction of riverlines. Magnification: 1K; Scale bar: 10μm
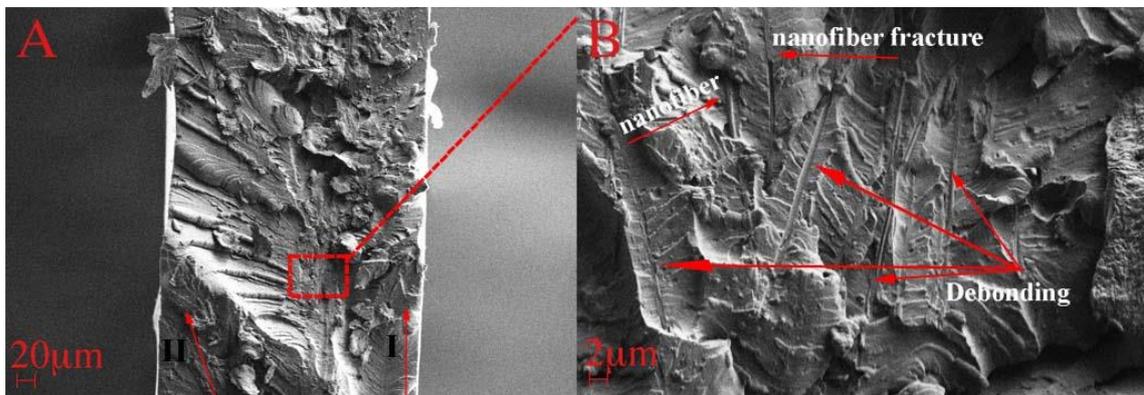
Figure 14 SEM image of PAN/epoxy laminated nanocomposite fracture surface, failed in tensile mode. A: Magnification: 500×; Scale bar: 20μm. B: Magnification: 5K; Scale bar: 2μm
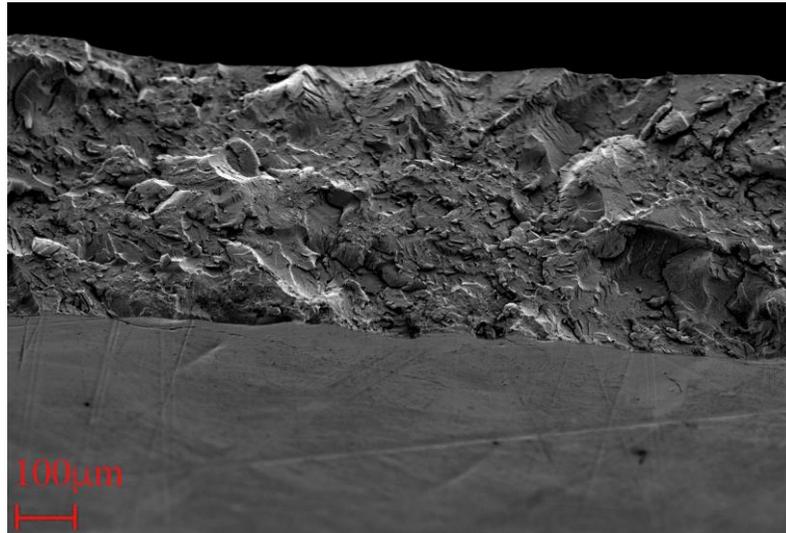
Figure 15 SEM image of PA6/ epoxy laminated nanocomposite fracture surface, failed under tensile load. Magnification: 100×; Scale bar: 100μm

3.4.3. Dynamic Mechanical Analysis (DMA) Results

Various test modes such as tensile, three point bending, dual cantilever, and single cantilever can be considered for nanocomposites in general [60,61,83–85]. However, application of tensile mode in the literature for polymeric nanofibrous nanocomposites seems to be rather limited [85,86]. This can partially be attributed to the difficulties in making properly sized representative DMA samples. For instance, thickness of manufactured nanocomposites with common techniques in the literature is likely to exceed maximum thickness allowed in a typical DMA testing [87]. In this work taking advantage of the proposed laminated nanocomposite manufacturing technique, tensile test specimens of X/epoxy, PA6/epoxy, PAN/epoxy, and PVB/epoxy samples were

molded with 20mm×5mm×0.5mm templates (according to Netzsch – DMA 242 C manual) and results of DMA are presented in Figure 16. As indicated in Figure 16 (A) the storage modulus (E') of the X nanofiber/epoxy laminated nanocomposite is equal to 3587±300 MPa at 25°C. This is 85% higher than the storage modulus of the neat epoxy 1938±400 MPa at the same temperature. Incorporation of PA6, PAN, and PVB nanofiber mat did not improved the storage modulus of neat epoxy samples as reported in Table 8 and Figure 16. Loss tangent (tanδ) curves known as the potential of the nanocomposite to dissipate energy (E''/E') [60,87] are presented in Figure 16 (B). X /epoxy nanocomposites resulted in the lowest loss tangent (tanδ) peak height in comparison to the neat epoxy. The loss tangent (tanδ) peak height of PA6/epoxy nanocomposite was also lower than neat epoxy. This is considered as an indication of nanofiber-matrix interface quality since dissipated energy in the interface region is product of the applied force and slipping displacement [60,88]. Loss tangent peak of PAN/epoxy laminated nanocomposite does not suggest promising fiber-matrix interface since it is only slightly below the damping peak of the neat epoxy nanocomposite. As a result PAN/epoxy laminated nanocomposites are expected to demonstrate brittle fracture with low toughness. PVB/epoxy laminated nanocomposite is the worst case with highest energy dissipation at fiber-matrix interface and consequently has the higher damping peak (tan δ) than neat epoxy nanocomposite. This observation from Figure 16(B) shows correlation with morphological analysis (SEM) of the PVB electrospun nanofiber mat and fiber-matrix interface at the processing temperature (140°C) covered in previous sections (3.4.1.1 and 3.4.1.2). Furthermore, the peak temperature of the loss tangent was considered as the glass transition temperature of nanocomposites. The glass

43

transition temperature of neat epoxy (135°C) was not altered by incorporation of nanofiber mats as the T_g for X/epoxy, PAN/epoxy, and PVB/epoxy were recorded 132°C, 134°C, and 132°C respectively. PA6/epoxy with tangent peak at 137°C was the only case with slightly improved T_g. Summary of the DMA analyses are reported in Table 8.
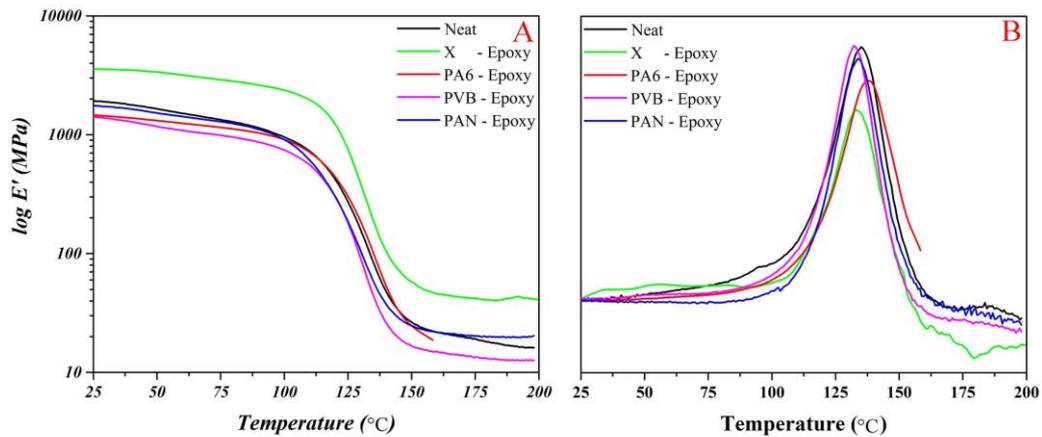
Figure 16 Dynamic mechanical analysis (DMA) of neat epoxy (3 epoxy film layers), X/epoxy, PA6/epoxy, PAN/epoxy, and PVB/epoxy laminated epoxy nanocomposites (2 mat/3 epoxy layers) in the tension mode. A: Log-scaled storage modulus scanned from 25°C up to 200°C. B: Loss tangent (tanδ) peak of neat epoxy and X/epoxy laminated nanocomposite.

Table 8 Results of the Dynamic Mechanical Analysis of neat epoxy and nanofiber/epoxy laminated nanocomposites tested in tension mode

Nanocomposite	E' (MPa)	Tg (°C)	Nanofiber wt (%)
Neat Epoxy	1938±400	135±2	-
X/ Epoxy	3587±300	132±2	1.1
PA6/ Epoxy	1465 ±300	137±2	1.1
PAN/ Epoxy	1768±350	134±2	1.1
PVB/ Epoxy	1417±300	132±2	1.1

3.5. Discussions

Nanofiber/epoxy matrix laminated nanocomposites are manufactured with a novel technique based on resin film molding and similar to prepreg technology. Incorporation of nanofiber veils as reinforcement in this technique reported to advantageous over nanofiller added solution casting as they disperse uniformly and eliminate agglomeration problems. Commercially available epoxy resin film and nanofibrous veils of Xantulayer (labeled as X), PA6, PAN, and PVB are used in order to highlight the scalability of the approach and reinforcing capabilities of different base polymers graded based on the their stand free properties and tensile behavior of the nanocomposites. Promising wettability measured with contact angle of the epoxy droplets with nanofibrous veils were reported for all reinforcement choices. However, SEM images of the standing-free mat epoxy film stacks of X, PA6, PAN, and PVB nanofibers followed by heat treatment at 140°C proved excellent nanofiber/epoxy adhesion for Xantulayer/epoxy and worst interface for PVB since nonwoven nanofibrous morphology were lost. Furthermore, SEM images of the nanofibrous mats heat treated at 140°C indicated that PVB nanofibers melt at the nanocomposite processing temperature while X, PA6, conserve their nanofibrous structure and only fraction of PAN

nanofibers with amorphous morphology soften. Tensile strength and stiffness of nanofiber mat from the highest to the lowest case are X, PAN, PA6, and PVB. The highest degree of cure (α) 0.96 and the lowest degree of cure (α) 0.68 were reported for X/epoxy and PAN/epoxy respectively while PA6 (with α= 0.92) and PVB (with α= 0.8) were in between. Laminated nanocomposites were tested on tensile (UTM and DMA). Integration of 1.1 wt% X nanofiber mat as the best case altered tensile strength, stiffness, and storage modulus (E') of neat epoxy by 25%, 9%, and 40% respectively. In-situ mechanical behavior of nanofiber/epoxy laminated nanocomposites was assessed by SEM based fracture surface analysis. Fracture surface of neat epoxy with river line dominated patterns and smooth morphology as typical features of brittle fracture were considered as reference for fracture surface analysis of X/epoxy nanocomposite with rough, fibrous region sandwiched between epoxy rich layers. Nanofiber exposure and corresponding debonding marks in the fracture surface of X/epoxy laminated nanocomposite were ascribed to high released energy upon failure. The PAN/epoxy demonstrated high stiffness 2932 Mpa comparable to X/epoxy with the lowest tensile strength 36 Mpa which might be ascribed to its low molecular weight (MW of nanofiber mats are kept as trade secret for PARDAM [62]). The nanofiber-epoxy interface analysis from DMA also suggested similar result with about the same loss tangent peak as neat epoxy. Various debonding marking on the fracture surface of the PAN/epoxy also is representative of high amount of released energy upon failure. PA6/epoxy laminated nanocomposites altered the stiffness by 18.7% and the tensile strength by 1.5% with respect to the neat epoxy. This improvement was also reflected in rough fracture morphology of PA6/epoxy. Although the storage modulus of the PA6/epoxy were lower than the virgin sample, good fiber-matrix interfacial properties were reported for the PA6/epoxy from loss tangent peak which is in coherence with its good wettability properties and tensile behavior. The incorporated PVB nanofibers had plasticizing effect (also reported in fracture surface analysis) with 10% improvement in failure strain of the neat sample, but the stiffness and strength were severely degraded. This observation is in agreement with the plastic like

46

fracture surface of PVB/epoxy, lowest tangent peak height of PVB/epoxy in DMA, and no improvement in the storage modulus.

CHAPTER 4

NANOFIBER/EPOXY LAMINATED NANOCOMPOSITES

4.1. Aim

In the previous chapter the proposed nanofiber/epoxy nanocomposite with uniform and controlled distribution of nanofiber veil impregnated into the epoxy matrix were emphasized as a mean to characterize the interlayer region (thin resin rich interlaminar domain interleaved with electrospun veils) in the laminated structural composites and the reinforcing potential of nanofibers based on different base polymers. In this chapter the focus is on the proposed film infusion method as a laminated nanocomposite making strategy and its scalability according to specific design in terms of number and configuration of reinforcing layer. Nanofiber/epoxy laminated nanocomposites comprised of 20 layers of X electrospun nanofiber mat and 21 layers of epoxy film much like conventional structural laminates (processed by the prepreg technology) are introduced in this chapter to elaborate on the scalability of the proposed approach. Regarding the excess number of epoxy resin films for these samples the processing steps are reported in more detail for completeness. High stiffness in bending and strength by incorporation of X nanofibrous veils with laminated microstructure were aimed. The processed X/epoxy laminated nanocomposites are tested with three point bending test (with UTM) and the laminated morphology of these nanocomposites are investigated by optical microscope.

4.2. Methodology

The laminated nanocomposites were manufactured following stablished steps in chapter 2 except some modification due to excess epoxy resin film fraction. A single layers of X nanofibrous veil and resin film (epoxy film/mat) were stacked on the aluminum caul plate until achieve the final configuration (20 layers of X mat and 21 layers of epoxy film). Due to excess number of epoxy resin films and the imposed air trap risk, after each 5 consecutive layers the lay-up were put into desiccator to remove the possible air

48

trap and then the surface were made sooth again by a roller as in Figure 17. These steps were multiplied until achieve 20 layers of X nanofibrous veil interleaved between 21 layers of epoxy resin film. The same specimen molding procedure established in chapter 2 was followed, but in accordance with ASTM D 790 – 02 to obtain samples of size 100 mm× 14.5 × 1.4mm. Once the stacking is done Figure 2C the open area between to aluminum caul-plates has been sealed to avoid the excessive flow of the resin during the cure cycle. Then, nanocomposite lay-up was vacuum bagged, placed into heating press and heated at a rate of 1°C/min up to 140°C without any applied pressure until 140°C. Nanocomposite was kept at 140°C for 1 hour while uniform pressure of 1 bar was maintained. Fiber weight fraction of the processed nanofiber/epoxy laminated nanocomposites was found to be 3.7%.
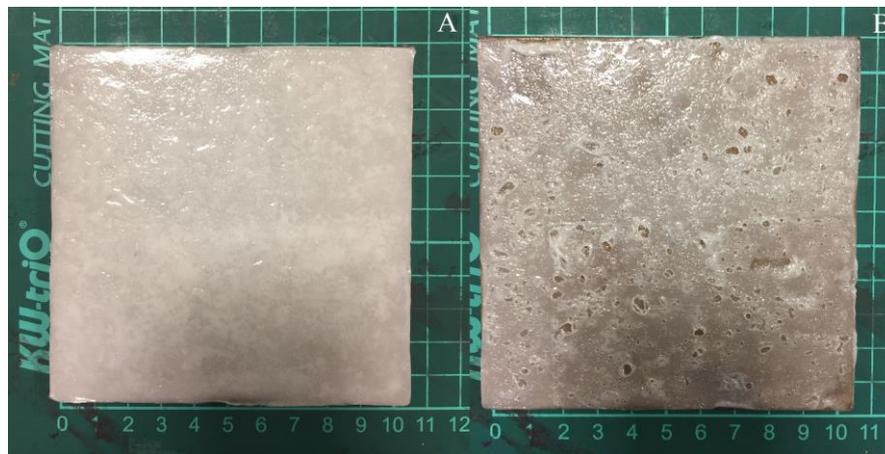
Figure 17 Removal of the air trap from epoxy lay-up into the desiccator. A: neat epoxy film layup in the pristine condition, B: neat epoxy lay-up vacuumed in the desiccator.

4.3.Discussions

Figure 18 already represented cross-section of the processed nanocomposites. It indicates that nanofibrous layers were infiltrated by epoxy. Note however, they are followed by a distinct neat epoxy layer for which the thickness varies through the overall thickness of the laminate. That is, there is a gradient of neat epoxy thickness through the thickness of the laminated nanocomposite. Results of the flexural tests are

49

reported in Figure 19A and Table 9. The epoxy samples with linearly elastic material behavior had ultimate flexural strength, flexural stiffness, and maximum flexural strain at 116 ± 13 MPa, 2953 ± 273 MPa, and $4.1\pm0.06\%$ respectly. These properties were improved by the incorporation of the X nanofiber which formed the reinforced laminated epoxy nanocomposites. Ultimate flexural strength, flexural stiffness, and flexural strain at failure of the laminated nanocomposite resulted as 135 ± 6 MPa, 4005 ± 168 MPa, and 5.2 ± 0.5 % respectly. It should be noted that although in polymeric composites increase in strength and stiffness is typically accompained by decrease in ductility, in the present X nanofiber reinforced laminated nanocomposite case improvement in ductility was also evident along with the significant improvement of in flexural stiffness and strength, 35.6 % and 16.4 %, respectively. As previously stated there is a gradient of neat epoxy layer thickness through the thickness of the laminated nanocomposite that can affect the flexural properties of the composite. This effect was assessed by the in-house code based on classical lamination theory (CLT). Neat epoxy and X/epoxy were took as two material input assigned for each distinctive layer and idealized as isotropic layers. Thickness of the layers was measured from five different regions to take thickness gradient into consideration. As an input elastic moduli (E) of neat epoxy and X/epoxy nanocomposite (extracted from tensile tests), G (in-plane shear modulus), poison ratio (ν), number and thickness of the consecutive layers were inserted in the code (G was due to the

Equation 1. Calculated in-plane stiffness matrix [A], flexural stiffness matrix [D] and coupling stiffness matrix [B] from CLT were normalized according to Equation 2 (Tsai, 1992, 2003, 2008). As reported in Table 10 the normalized in-plane and flexural stiffness matrices A_{ij}^* and D_{ij}^* are very close to each other and coupling stiffness matrix B_{ij}^* is non-zero, but small. These suggest a homogenized X/epoxy laminated nanocomposite. The average normalized stiffness D_{11}^* of nanocomposite from CLT is 3200 MPa which is below the measured flexural stiffness 4000 MPa from three points bending test.

Equation 1 $G = \dfrac{E}{2(1+\nu)}$

Equation 2 $[A^*] = 1/h\ [A],\ [B^*] = 2/h^2\ [B]\ [D^*] = 12/h^3\ [D]$
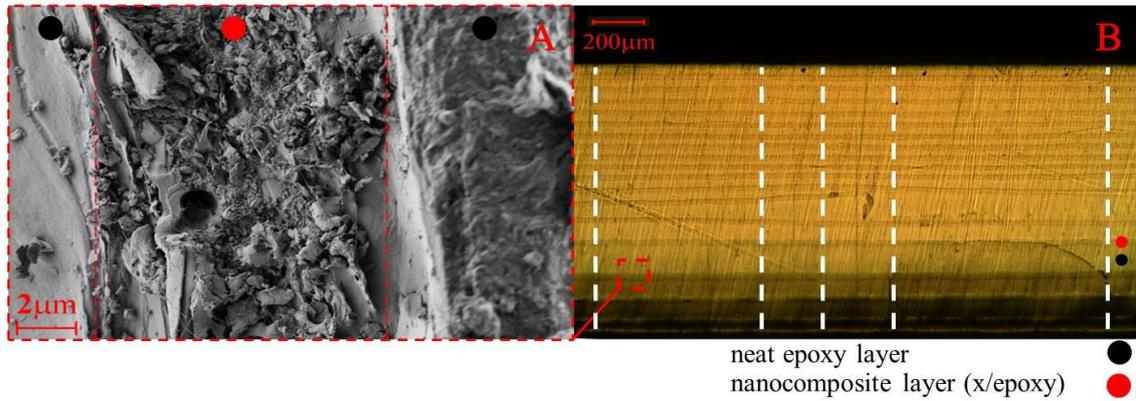
Figure 18 Cross-section of the nanofiber reinforced laminated epoxy nanocomposite. (B) Optic microscope image of the nanofiber reinforced epoxy nanocomposite. Scale bar: 200 μm (A) SEM image of the fiber-matrix interface in the nanocomposite. Scale bar: 2μm. Epoxy matrix is indicated by black circles and nanocomposites (epoxy infused nanofiber veils) by red circles. Dashed lines in the figure B from left to right are L_1, L_2, L_3, L_4, and L_5 which have been used in CLT calculations.
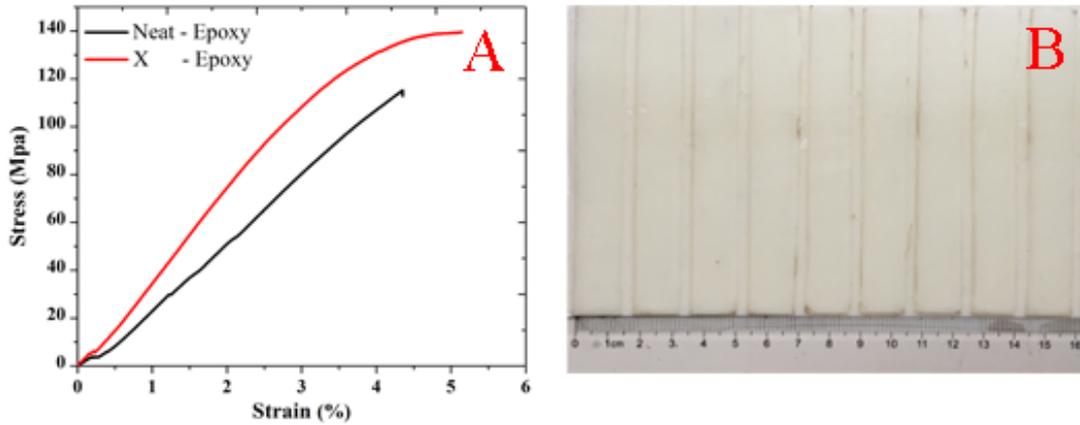
Figure 19 Flexural stress-strain analysis (UTM) of the neat epoxy nanocomposite with 21 layers of epoxy resin film, and X nanofiber reinforced laminate epoxy nanocomposite with 20 layers of X nanofiber mat and 21 layers of epoxy resin film with average X nanofiber weight fraction of 3.7.

Table 9 Results of the three point bending test for neat epoxy samples and X/epoxy laminated nanocomposites

Sample / Mechanical testing mode	# of epoxy layers	# of reinforcing layers	Fiber wt (%)	Stiffness (MPa)	Failure strength (MPa)	Flexural strain at failure (%)
Neat epoxy	21	0	0	2953± 273	116±13	4.1
X/epoxy	21	20	3.7	4005±168	135±6	5.2

Table 10 Normalized in-plane and flexural stiffness matrices measured from five distinct regions in the cross-section image of the X/epoxy laminated nanocomposite

Measured region	[A*] MPa			[D*] MPa			[B*] MPa		
	A11*	A12*	A16*	D11*	D12*	D16*	B11*	B12*	B16*
	A12*	A22*	A26*	D12*	D22*	D26*	B12*	B22*	B26*
	A61*	A62*	A66*	D61*	D62*	D66*	B61*	B62*	B66*
Line 1	3241	1134	0	3237	1133	0	-14.3	-5	0

	1134	3241	0	1133	3237	0	-5	-14.3	0
	0	0	1052	0	0	1051	0	0	-4.6
Line 2	3241	1134	0	3248	1136	0	-12.2	-4.2	0
	1134	3241	0	1136	3248	0	-4.5	-12.3	0
	0	0	1053	0	0	1055	0	0	-4.2
Line 3	3232	1131	0	3232	1130	0	-12.3	-4.3	0
	1131	3232	0	1130	3230	0	-4.3	-12.2	0
	0	0	1050	0	0	1049	0	0	-4
Line 4	3227	1130	0	3237	1133	0	-14	-5	0
	1130	3227	0	1133	3237	0	-4.9	-14	0
	0	0	1048	0	0	1051	0	0	-4.6
Line 5	3325	1163	0	3312	1159	0	-12.4	-4.3	0
	1163	3325	0	1159	3312	0	-4.3	-12.4	0
	0	0	1080	0	0	1078	0	0	-4

CHAPTER 5
BACK CALCULATING MECHANICAL PROPERTIES AND MATERIAL MODEL OF ELECTROSPUN NANOFIBERS BASED ON EXPERIMENTAL BEHAVIOR OF NANOCOMPOSITES AND MEAN FIELD HOMOGENIZATION

5.1. Overview

The potential of the proposed nanofiber/epoxy nanocomposite processing technique was discussed in the previous chapters. Once the experimental data (e.g. tensile properties) of representative nanofiber reinforced nanocomposites along with the neat epoxy data are available, the material models of the constituents can be assessed to back calculate individual nanofiber modulus that best fit the experimental nanocomposite data. Electrospun nanofiber mats of X, PA6, PAN, and PVB were studied by the associated capability of the Digimat software. Mean-field homogenization (MFH) method based on Mori-Tanaka [89] is one of the key cababilities of Digimat-MF as scale-transition method (micro to macro, Eshelby's single inclusion solution). Electrospun polymeric nanofiber mats were presumed elastic and modeled ad 2D random distribution within epoxy matrix. Epoxy was both alternatively as elastoplastic and elastic. After the homogenization, an iterative optimization process is carried out in Digimat-MX software to find the presumed material model parameters or Continuous Design Variables (CVD) that minimize the difference between the Digimat Analysis and experimental results. Details on the homogenization method, employed material models, and optimization process are reported in appendix.

5.2.Results and Discussion

Stress-strain behavior of the neat epoxy samples is examined prior to nanofiber/epoxy laminated nanocomposites as it comprises the matrix phase for nanocomposites. The experimental stress-strain behavior of the neat epoxy samples depicted in Figure 7 shows non-linear elastic behavior but the Digimat-MX software version available for this thesis is only capable of modeling Linear-Elasticity. To achieve the best fit with tensile experimental data, linear elasticity Figure 20 and elastoplasticity Figure 21 material models as two case studies were assessed. The result of the back calculation for the neat epoxy with elastoplastic material model completely fitted on the experimental data so it would be employed in back calculating elastic modulus of X Figure 22, PA6 Figure 23, PAN Figure 24, and PVB single nanofibers. Electrospun nanofiber mats are assumed linear elastic with random 2D distribution and aspect ratio of 1000 embedded in the elastoplastic epoxy resin. The calculated curve fits between the experimental tensile curve and the mean field homogenization analyses (MFH) for X/epoxy, PA6/epoxy, and PAN/epoxy were promising. As incorporation of PVB nanofiber mats degraded the tensile behavior of neat epoxy the Digimat-MX was unable to predict this behavior. The predicted elastic moduli of X (PA66 based nanofiber as reported in [19]), PA6, and PAN single nanofibers are 22.4 GPa, 20.9 GPa, and 49.3 GPa as recorded in Table 11. The elastic modulus of PAN single nanofiber is close to the experimental elastic modulus 48 GPa as reported in [90]. The elastic moduli of X and PA6 single nanofibers reported herein are one order of magnitude higher than the reported elastic modulus (measured by AFM and SEM) such as that reported by Hang, et.al (1.32 $\pm$ 0.152GPa)[91].
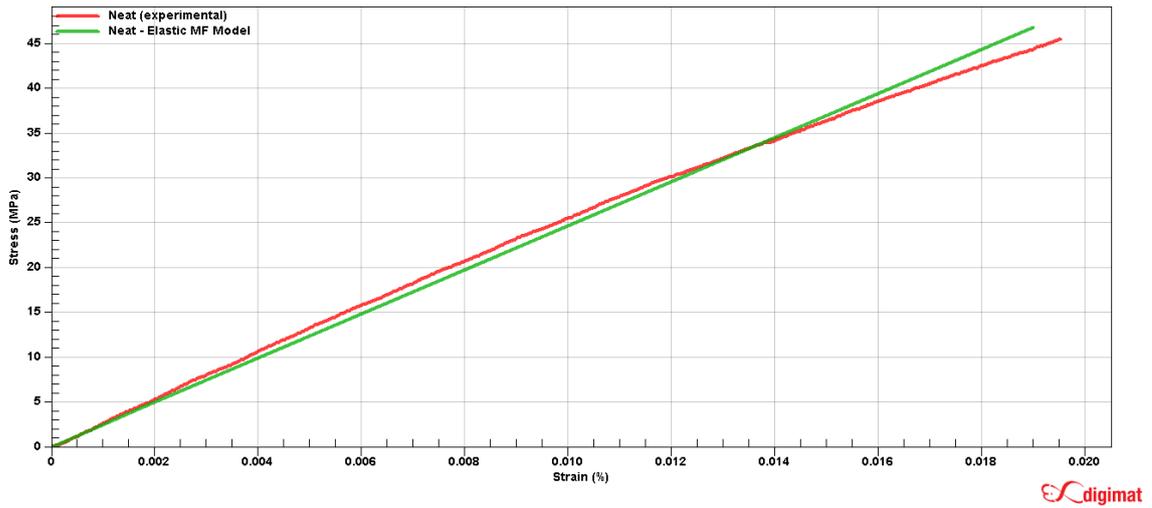
Figure 20 Back calculation of tensile behavior of the neat epoxy with linear elastic material model (green curve) with reference to the experimental tensile behavior of neat epoxy (red curve)
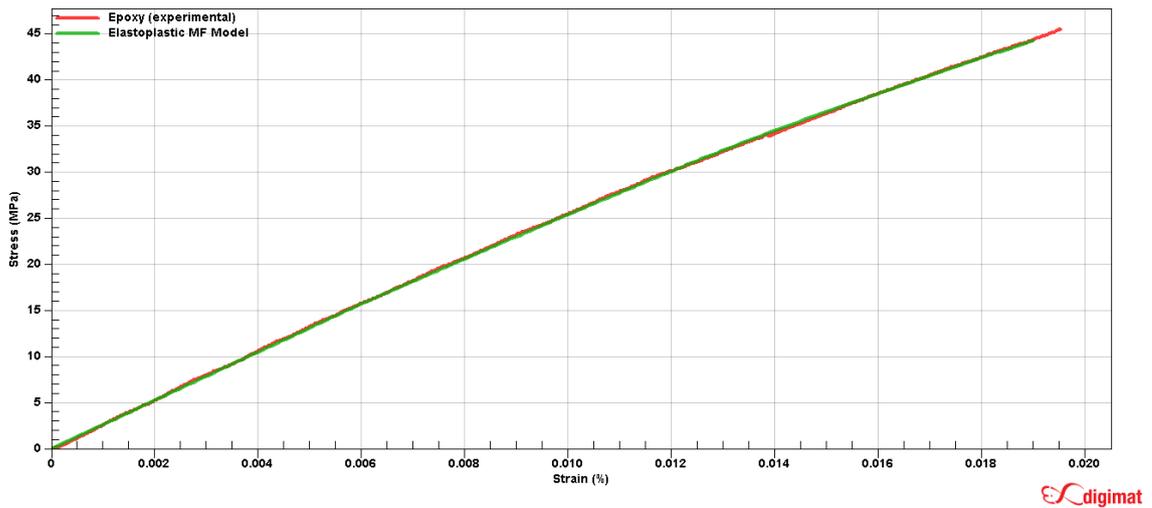
Figure 21 Back calculation of tensile behavior of the neat epoxy with elastoplastic material model (green curve) with reference to the experimental tensile behavior of neat epoxy (red curve)
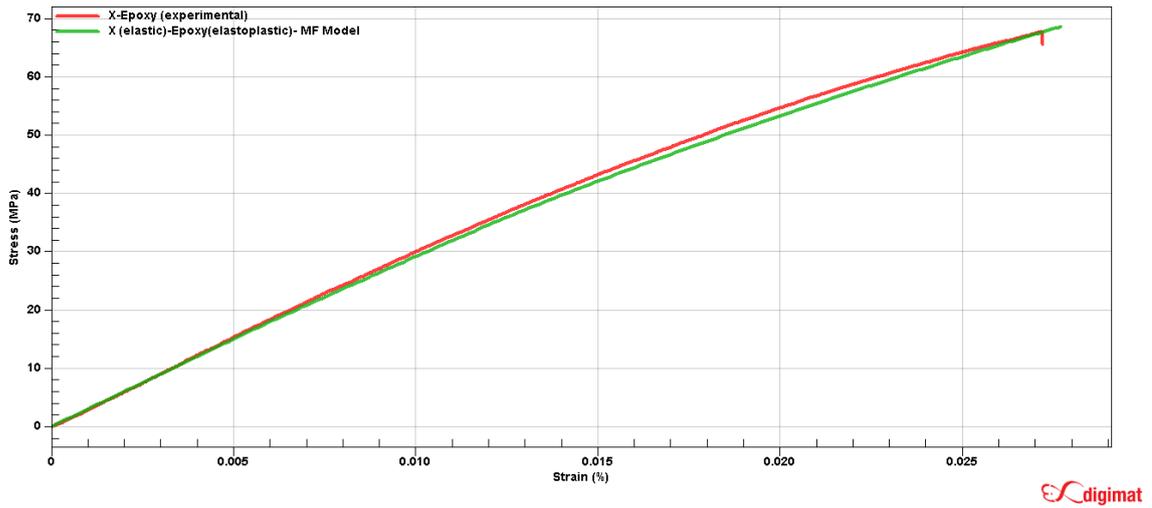
Figure 22 Back calculation of tensile behavior of the X/epoxy laminated nanocomposite. X nanofibers are assumed elastic and randomly distributed in 2D; epoxy matrix phase is modeled via elastoplastic material model (green curve) with reference to the experimental tensile behavior of X/epoxy laminated nanocomposite (red curve)
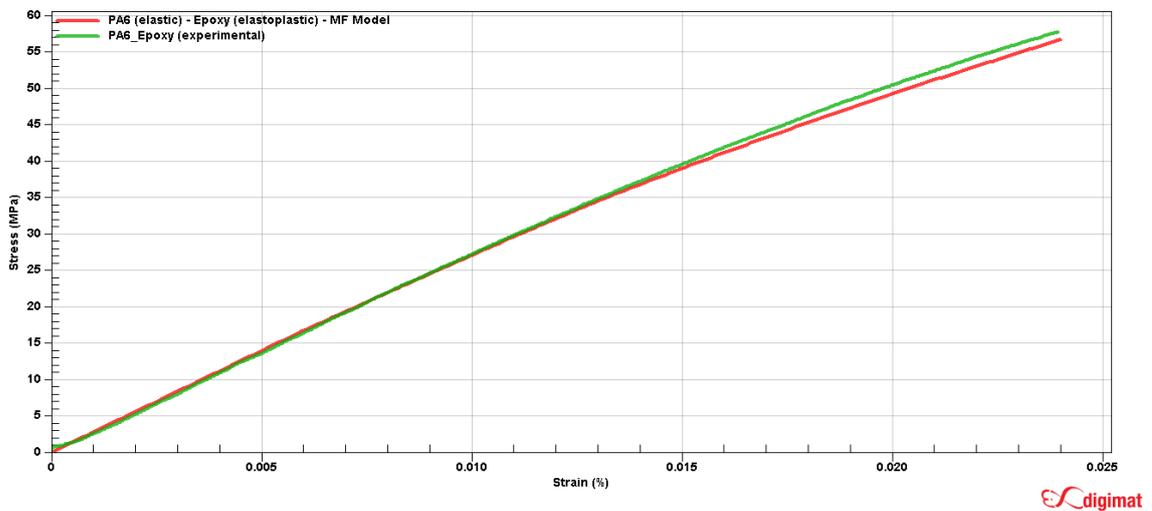
Figure 23 Back calculation of tensile behavior of the PA6/epoxy laminated nanocomposite. PA6 nanofibers are assumed elastic and randomly distributed in 2D; epoxy matrix phase is modeled via elastoplastic material model (green curve) with

reference to the experimental tensile behavior of PA6/epoxy laminated nanocomposite (red curve)
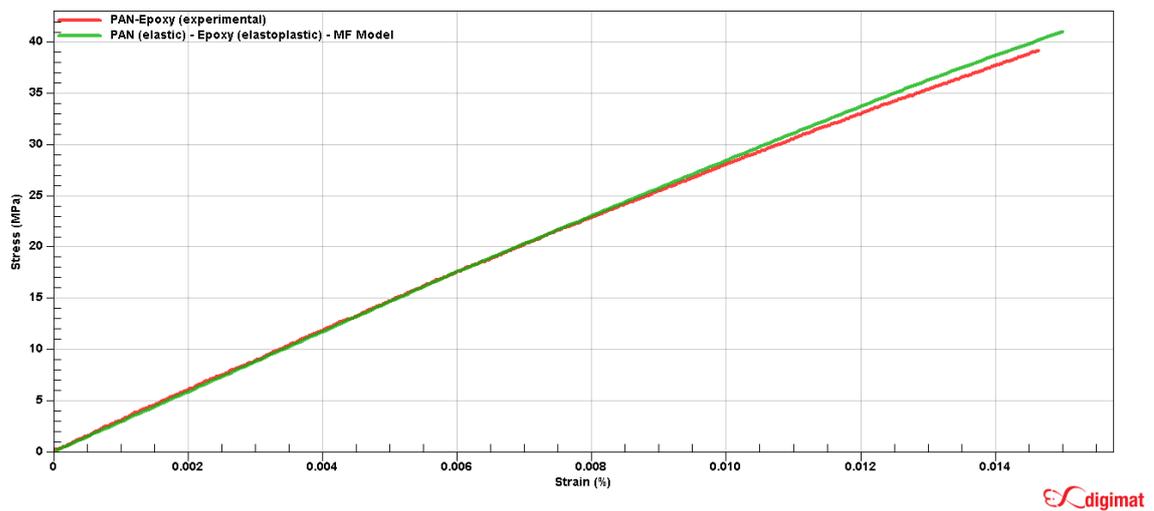
Figure 24 Back calcuation of tensile behavior of the PAN/epoxy laminated nanocomposite. PAN nanofibers are assumed elastic and randomly distributed in 2D, epoxy matrix phase is modeled via elastoplastic material model (green curve) with reference to the experimental tensile behavior of PAN/epoxy laminated nanocomposite (red   curve)

Table 11 Material model, and elastic modulus of the neat epoxy resin and X, PA6, PAN single nanofibers

Nanocomposite	Nanofiber material model	Matrix material model	Elastic modulus (MPa)	Yield strength (MPa)	H.M	E.M
Neat	-	linear elastic	2463.49	-	-	-
Neat	-	elastoplastic	2628	15.8	455.8	0.45
X/epoxy	linear elastic/ random 2D	elastoplastic	22439 (single X nanofiber)	-	-	-
PA6/epoxy	linear elastic/ random 2D	elastoplastic	20938 (single PA6 nanofiber)	-	-	-
PAN/epoxy	linear elastic/ random 2D	elastoplastic	49353 (single PAN nanofiber)	-	-	-

CHAPTER 6

FUTURE WORKS

In this thesis work electrospun nanofiber veils based on different base polymers were employed as the reinforcement choices with uniform and controlled distribution of nanofiber mats. The scalability of the proposed nanocomposite manufacturing method based on resin film infusion were proved with processing nanofiber/epoxy laminated nanocomposites with 20 layers of nanofiber mats interleaved between 20 layers of epoxy resin film. These two attributes could be the building block for the future works in tuning nanofiber/epoxy laminated nanocomposite with different base polymers adjusted on each layer based on nanocomposite design. This could be advantageous in design process of the structural laminated nanocomposites as the proposed nanofiber/epoxy laminated nanocomposites could be sought as the representative nanocomposite layer in the interlaminar region. As reported in chapter 5 coupling these representative nanocomposites with Finite Element Analysis (FEA) the mechanical properties of a single nanofiber could be back calculated. However, further studies such as efforts including morphology and microstructure based homogenizations and representative experimental data are needed as the results were not consistently validated. Development of such a validated scheme, not only for stiffness but also strength could be helpful for FEA based fracture mechanics and failure predictions in nanofiber interleaved laminated composites.

6. Appendix

6.1. Material Models

6.1.1. Isotropic Linear Elasticity

Electrospun nanofiber mats of X, PA6, PAN, and PVB are assumed as thermoplastic with isotropic linear elastic material model (which makes material properties independent of the loading direction) and random 2D distribution. As in Equation 4 the isotropic Young's modulus and Poisson's ratio are sufficient for characterization of Hooke's operator denoted by C in Equation 3 known as Hook's law. Shear and bulk moduli could be extracted according to

Equation 3 $\sigma = C\varepsilon$

Equation 4

$$S^{el} = \frac{1}{E} \begin{bmatrix} 1 & -\nu & -\nu & 0 & 0 & 0 \\ & 1 & -\nu & 0 & 0 & 0 \\ & & 1 & 0 & 0 & 0 \\ & & & 2(1+\nu) & 0 & 0 \\ & sym. & & & 2(1+\nu) & 0 \\ & & & & & 2(1+\nu) \end{bmatrix}.$$

Equation 5 $G = \dfrac{E}{2(1+\nu)}$ and $K = \dfrac{E}{3(1-2\nu)}$

6.1.2. Elastoplasticity with J₂ plasticity model

The elastoplastic behavior definition in Digimat-MF is based on Huber-Mises-Hencky (HMH) criteria as the material begins to deform plastically as the stress intensity in the material reaches the value of yield strength Figure 25. This model is known as the J_2 – plasticity model based on the von Mises equivalent stress $J_2(\sigma)$ defined in Equation 6 with upper bound for linear elasticity defined in Equation 7 with total strain defined as $(\varepsilon = \varepsilon^e + \varepsilon^p)$.

Equation   6

$$J_2\,(\sigma) \;=\; \left(\frac{0.75}{2}[(\sigma_{11}\text{-}\sigma_{22})^2 \;+\; (\sigma_{11}\text{-}\ \sigma_{33})^2 \;+\; (\sigma_{33}\text{-}\sigma_{11})^2] \;+\; 3[\sigma_{12}{}^2 \;+\; \sigma_{23}{}^2 \;+\; \sigma_{31}{}^2\ ]\right)^{1/2}$$

Equation   7 J_2 (σ) $\leq$ σ_y

The Cauchy stress and the elastic strain are then related by: $\sigma = C: \varepsilon^e$, where C: Hook's operator. If $J_2\,(\sigma) > \sigma_y$ the response becomes nonlinear and plastic deformation appears. Then the Cauchy stress obeys $\sigma_{eq} = \sigma_Y + R\,(p)$ where R (p) is the hardening stress and p the accumulated plastic strain expressed as in Equation 8. Yield function f (σ, R) could be written as in Equation 9. The material behaves as an elastic part if f $(\sigma, R) < 0$, otherwise the material is in the plastic domain. The extension of the plastic strain tensor ε^p is given in Equation 10. Power law and exponential law as the isotropic hardening models are given in Equation 11 and Equation 12 respectively.

Equation 8 $p\,(t) = \int_0^t \dot{p}\,(\tau)\,d\,\tau$ where $\dot{p} = (\frac{2}{3}\,\dot{\varepsilon}^p : \dot{\varepsilon}^p)^{1/2}$,

Equation 9 $f(\sigma,R) = J_2(\sigma) - \sigma_Y - R(p) \leq 0$,

Equation 10 $\dot{\varepsilon}_p = \dot{p}\,\dfrac{\partial f}{\partial \sigma}$,

Equation 11 R (p) = kp^m, (for horizontal stress-strain plateau)

Equation 12 R (p) = R_∞[1-exp (-mp)], (for plateau almost reached but the stress level keeps   increasing   slowly)
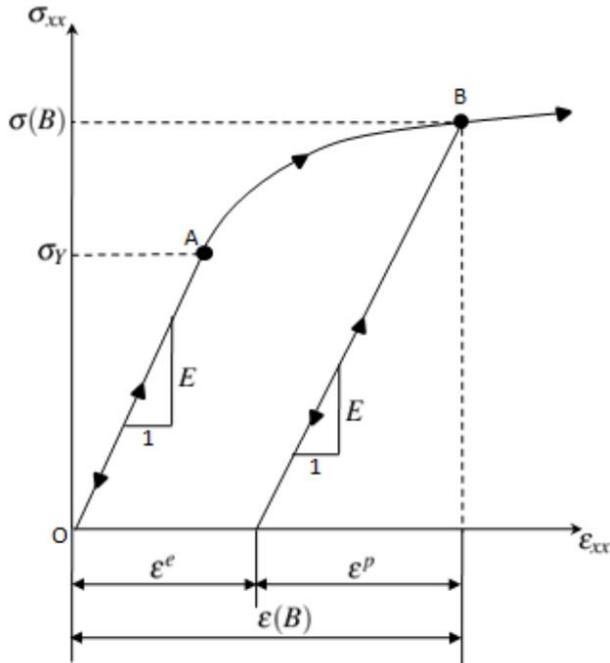
Figure 25 idealized stress-strain behavior of a polymer under uniaxial tension in the x-direction

6.2. Homogenization and Back Calculation

Mean-field homogenization (MFH) method based on Mori-Tanaka [89] is the cornerstone of Digimat-MF as scale-transition method (micro to macro) which aims to estimates the volume averages of the stress and strain fields at the RVE level (macro stresses and strains) and in each phase. For a two phase composites with matrix and inclusion denoted by 0 and 1 subscripts respectively, the volume averages of the strain field over the Representative Volume Element (RVE) relates the matrix and inclusion phases as depicted in Equation 13,Equation 14, and Equation 15. In Equation 15 the

volume average of strain over all inclusions is related to the volume average via the first tensor and to the volume average of strain over the entire RVE (macro strain) with the second tensor.

Equation 13: $v_0 + v_1 = 1$

Equation 14: $<\varepsilon> w = v_0 <\varepsilon> w_0 + v_1 <\varepsilon> w1$, w: domain

Equation 15: $<\varepsilon> w_1 = B^\varepsilon : <\varepsilon> w_0, <\varepsilon> w_1 = A^\varepsilon : <\varepsilon> w$ (strain concentration tensor for MFH definition)
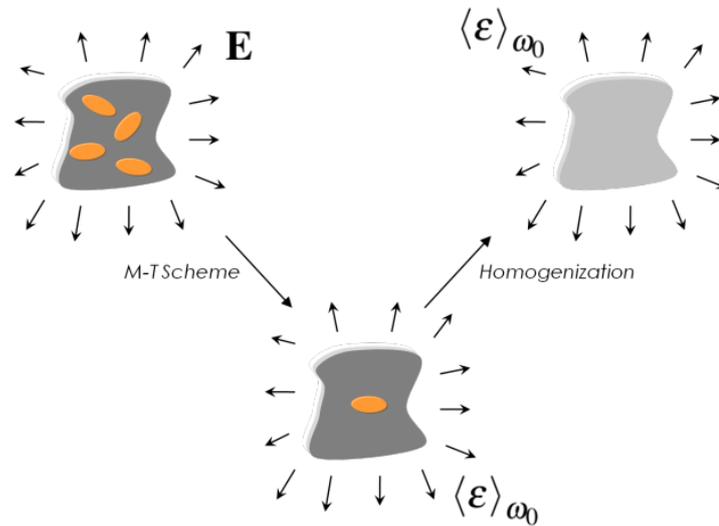
Figure 26 Schematic of Mori-Tanka Method

In the homogenization process, the Eshelby's tensor is required to compute the strain concentration tensor "B" in Equation 16 where I: fourth-rank identity tensor, ζ Eshelby's tensor, P Hill's or polarization tensor, C_0 and C_1 the stiffness matrices of the matrix and equivalent inclusion phases.

Equation 16: $B^\varepsilon = \{I + \zeta : C_0^{-1}:[C1 - C0]\}^{-1} = \{I + P : [C1 - C0]\}^{-1}$

Dividing RECTangles (DIRECT) [92] an optimization algorithm from the COLINY methods in DAKOTA [93] used by Digimat. MX.6.1.1 program is employed for back calculation the material models and constituent properties. DIRECT is a derivative free global optimization technique that balances local search in promising regions of the design space with the global search in unexplored regions. Prior knowledge of the objective function is not required since it is a sampling algorithm and adaptively subdivides the space of the feasible design points so as to guarantee that iterates are generated around a global minimum Figure 27.
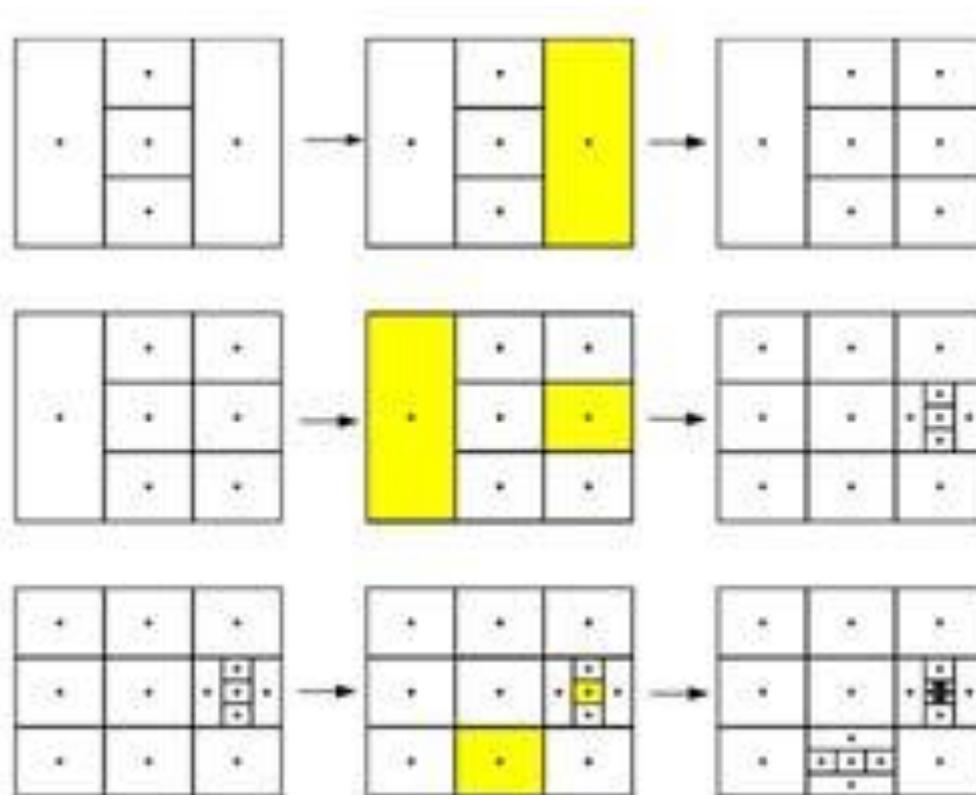
Figure   27   Design   space   Portioning   with   DIREKT

65

References

[1]   Production of nanofibers by melt spinning. US Pat 2012.

[2]   Yoon Y, Baik H. Catalytic growth mechanism of carbon nanofibers through chemical vapor deposition. Diam Relat Mater 2001.

[3]   Lin Y, Yao Y, Yang X, Wei N, Li X. Preparation of poly (ether sulfone) nanofibers by gas-jet/electrospinning. J Appl 2008.

[4]   Zhang S. Fabrication of novel biomaterials through molecular self-assembly. Nat Biotechnol 2003.

[5]   Kannan B, Cha H, Hosie I. Electrospinning—Commercial Applications, Challenges and Opportunities. Nano-Size Polym 2016.

[6]   Taylor G. Disintegration of water drops in an electric field. Proc R Soc 1964.

[7]   Reneker D, Yarin A. Electrospinning jets and polymer nanofibers. Polymer (Guildf) 2008.

[8]   Cai Y, Gevelber M. The effect of relative humidity and evaporation rate on electrospinning: fiber diameter and measurement for control implications. J Mater Sci 2013.

[9]   Beachley V, Wen X. Effect of electrospinning parameters on the nanofiber diameter and length. Mater Sci Eng C 2009;29:663–8. doi:10.1016/j.msec.2008.10.037.

[10]   Yalcinkaya B, Yener F, Jirsak O. On the nature of electric current in the electrospinning process. J 2013.

[11]   Yener F, Yalcinkaya B, Jirsak O. On the measured current in needle-and needleless electrospinning. J Nanosci 2013.

[12]   Thompson CJ, Chase GG, Yarin AL, Reneker DH. Effects of parameters on nanofiber diameter determined from electrospinning model. Polymer (Guildf) 2007;48:6913–22. doi:10.1016/j.polymer.2007.09.017.

[13]   Gupta P, Elkins C, Long T, Wilkes G. Electrospinning of linear homopolymers of poly (methyl methacrylate): exploring relationships between fiber formation, viscosity, molecular weight and concentration. Polymer (Guildf) 2005.

[14]   Koski A, Yim K, Shivkumar S. Effect of molecular weight on fibrous PVA produced by electrospinning. Mater Lett 2004.

[15]   BIOINICIA ELECTROSPINNING ELECTROSPRAYING FLUIDNATEK n.d. http://www.bioinicia.com/ (accessed July 17, 2017).

[16]   Jirsak O, Sanetrnik F, Lukas D, Kotek V. Method of nanofibres production from a polymer solution using electrostatic spinning and a device for carrying out the method. US Pat 2009.

[17]   Revolution Fibres n.d. http://www.revolutionfibres.com/ (accessed July 17, 2017).

[18]   Elmarco │ Nanospider^{TM} equipment n.d. http://www.elmarco.com/ (accessed July 17, 2017).

[19]   Beckermann G. Nanofiber interleaving veils for improving the performance of composite laminates. Reinf Plast 2017.

[20]   O'Brien T. Towards a damage tolerance philosophy for composite materials and structures. Compos Mater Test Des (Ninth 1990.

[21]   Zucchelli A, Focarete ML, Gualandi C, Ramakrishna S. Electrospun nanofibers for enhancing structural performance of composite materials. Polym Adv Technol 2011;22:339–49. doi:10.1002/pat.1837.

[22]   Brugo TM, Minak G, Zucchelli A, Saghafi H, Fotouhi M. An Investigation on

the Fatigue based Delamination of Woven Carbon-epoxy Composite Laminates Reinforced with Polyamide Nanofibers. Procedia Eng 2015;109:65–72. doi:10.1016/j.proeng.2015.06.208.

[23]   Daelemans L, van der Heijden S, De Baere I, Rahier H, Van Paepegem W, De Clerck K. Improved fatigue delamination behaviour of composite laminates with electrospun thermoplastic nanofibrous interleaves using the Central Cut-Ply method. Compos Part A Appl Sci Manuf 2017;94:10–20. doi:10.1016/j.compositesa.2016.12.004.

[24]   HOJO M, ANDO T, TANAKA M, ADACHI T, OCHIAI S, ENDO Y. Modes I and II interlaminar fracture toughness and fatigue delamination of CF/epoxy laminates with self-same epoxy interleaf. Int J Fatigue 2006;28:1154–65. doi:10.1016/j.ijfatigue.2006.02.004.

[25]   Ghiasi H, Fayazbakhsh K, Pasini D, Lessard L. Optimum stacking sequence design of composite materials Part II: Variable stiffness design. Compos Struct 2010;93:1–13. doi:10.1016/j.compstruct.2010.06.001.

[26]   Wu C, Viquerat A. Natural frequency optimization of braided bistable carbon/epoxy tubes: Analysis of braid angles and stacking sequences. Compos Struct 2017;159:528–37. doi:10.1016/j.compstruct.2016.09.075.

[27]   Kishi H, Kuwata M, Matsuda S, Asami T, Murakami A. Damping properties of thermoplastic-elastomer interleaved carbon fiber-reinforced epoxy composites. Compos Sci Technol 2004;64:2517–23. doi:10.1016/j.compscitech.2004.05.006.

[28]   Nagendra S, Haftka R, Gürdal Z. Stacking sequence optimization of simply supported laminates with stability and strain constraints. AIAA J 1992.

[29]   Soremekun G, Gürdal Z, Kassapoglou C, Toni D. Stacking sequence blending of multiple composite laminates using genetic algorithms. Compos Struct 2002.

[30]   Sharma SK, Sankar B V. Sublaminate Buckling and Compression Strength of

Stitched Uniweave Graphite/Epoxy Laminates. J Reinf Plast Compos 1997;16:425–34. doi:10.1177/073168449701600503.

[31] Chan WS, Ochoa OO. Edge Delamination Resistance by a Crictical Ply Termination. Key Eng Mater 1989;37:285–304. doi:10.4028/www.scientific.net/KEM.37.285.

[32] Carolan D, Ivankovic A, Kinloch AJ, Sprenger S, Taylor AC. Toughened carbon fibre-reinforced polymer composites with nanoparticle-modified epoxy matrices. J Mater Sci 2017;52:1767–88. doi:10.1007/s10853-016-0468-5.

[33] Kamar.Nicholas T DLT. Nanoscale toughening of carbon fiber reinforced/epoxy polymer composites (CFRPs) using a triblock copolymer - ScienceDirect. Polymer (Guildf) 2017;111:36–47. doi:https://doi.org/10.1016/j.polymer.2017.01.009.

[34] Kuwata M. HPJ. Interlaminar toughness of interleaved CFRP using non-woven veils: Part 1. Mode-I testing - ScienceDirect. Compos Part A 2011;42:1551–9.

[35] Beckermann GW, Pickering KL. Mode I and Mode II interlaminar fracture toughness of composite laminates interleaved with electrospun nanofibre veils. Compos Part A Appl Sci Manuf 2015;72:11–21. doi:10.1016/j.compositesa.2015.01.028.

[36] Tsotsis TK. Interlayer toughening of composite materials. Polym Compos 2009;30:70–86. doi:10.1002/pc.20535.

[37] Dzenis Y. Structural Nanocomposites. Science (80-) 2008;319.

[38] Kim J, Reneker D. Mechanical properties of composites using ultrafine electrospun fibers. Polym Compos 1999.

[39] Dzenis Y, Reneker D. Delamination resistant composites prepared by small diameter fiber reinforcement at ply interfaces. US Pat 6,265,333 2001.

[40] Bilge K, Ozden-Yenigun E, Simsek E, Menceloglu YZ, Papila M. Structural composites hybridized with epoxy compatible polymer/MWCNT nanofibrous interlayers. Compos Sci Technol 2012;72:1639–45. doi:10.1016/j.compscitech.2012.07.005.

[41] Özden-Yenigün E, Bilge K, Sünbüloğlu E, Bozdağ E, Papila M. High strain rate response of nanofiber interlayered structural composites. Compos Struct 2017;168:47–55. doi:10.1016/j.compstruct.2017.02.007.

[42] Heijden S van der, Daelemans L. Interlaminar toughening of resin transfer moulded glass fibre epoxy laminates by polycaprolactone electrospun nanofibres. Sci Technol 2014.

[43] van der Heijden S, Daelemans L, De Bruycker K, Simal R, De Baere I, Van Paepegem W, et al. Novel composite materials with tunable delamination resistance using functionalizable electrospun SBS fibers. Compos Struct 2017;159:12–20. doi:10.1016/j.compstruct.2016.09.057.

[44] Brugo T, Palazzetti R. The effect of thickness of Nylon 6,6 nanofibrous mat on Modes I–II fracture mechanics of UD and woven composite laminates. Compos Struct 2016;154:172–8. doi:10.1016/j.compstruct.2016.07.034.

[45] SAGHAFI H, PALAZZETTI R, MINAK G, ZUCCHELLI A. EFFECT OF PAN NANOfiBER INTERLEAVING ON IMPACT DAMAGE RESISTANCE OF GFRP LAMINATES. nanocon2013.tanger.cz n.d.

[46] Bilge K, Venkataraman S, Menceloglu YZ, Papila M. Global and local nanofibrous interlayer toughened composites for higher in-plane strength. vol. 58. 2014. doi:10.1016/j.compositesa.2013.12.001.

[47] Liao H, Wu Y, Wu M, Zhan X, Liu H. Aligned electrospun cellulose fibers reinforced epoxy resin composite films with high visible light transmittance. Cellulose 2012;19:111–9. doi:10.1007/s10570-011-9604-1.

[48] Electrospun nylon nanofibers as effective reinforcement to polyaniline membranes. Mater Interfaces 2009.

[49] Jiang S, Duan G, Hou H, Greiner A, Agarwal S. Novel Layer-by-Layer Procedure for Making Nylon-6 Nanofiber Reinforced High Strength, Tough, and Transparent Thermoplastic Polyurethane Composites. ACS Appl Mater Interfaces 2012;4:4366–72. doi:10.1021/am3010225.

[50] Sancaktar E, Aussawasathien D. Nanocomposites of Epoxy with Electrospun Carbon Nanofibers: Mechanical Behavior. J Adhes 2009;85:160–79. doi:10.1080/00218460902881758.

[51] Özden-Yenigün E, Menceloğlu YZ, Papila M. MWCNTs/P(St- *co* -GMA) Composite Nanofibers of Engineered Interface Chemistry for Epoxy Matrix Nanocomposites. ACS Appl Mater Interfaces 2012;4:777–84. doi:10.1021/am2014162.

[52] Kim J, Reneker DH. Mechanical properties of composites using ultrafine electrospun fibers. Polym Compos 1999;20:124–31. doi:10.1002/pc.10340.

[53] Liao H, Wu Y, Wu M, Liu H. Effects of fiber surface chemistry and roughness on interfacial structures of electrospun fiber reinforced epoxy composite films. Polym Compos 2011;32:837–45. doi:10.1002/pc.21107.

[54] Stachewicz U, Modaresifar F, Bailey R. Manufacture of void-free electrospun polymer nanofiber composites with optimized mechanical properties. Appl Mater … 2012.

[55] Jana S, Jain S. Dispersion of nanofillers in high performance polymers using reactive solvents as processing aids. Polymer (Guildf) 2001.

[56] Hussain F, Hojjati M, Okamoto M. Review article: polymer-matrix nanocomposites, processing, manufacturing, and application: an overview. J Compos 2006.

[57] Rana S, Alagirusamy R, Joshi M. Effect of carbon nanofiber dispersion on the tensile properties of epoxy nanocomposites. J Compos Mater 2011;45:2247–56. doi:10.1177/0021998311401076.

[58] Liao Y, Marietta-Tondin O, Liang Z, Zhang C. Investigation of the dispersion process of SWNTs/SC-15 epoxy resin nanocomposites. Mater Sci 2004.

[59] Kim J, Seong D, Kang T, Youn J. Effects of surface modification on rheological and mechanical properties of CNT/epoxy composites. Carbon N Y 2006.

[60] Ozden E, Menceloglu Y, Papila M. Engineering chemistry of electrospun nanofibers and interfaces in nanocomposites for superior mechanical properties. ACS Appl Mater 2010.

[61] De Schoenmaker B, Van der Schueren L, Ceylan Ö, De Clerck K, De Schoenmaker B, Van der Schueren L, et al. Electrospun Polyamide 4.6 Nanofibrous Nonwovens: Parameter Study and Characterization. J Nanomater 2012;2012:1–9. doi:10.1155/2012/860654.

[62] Pardam | "We make nanofibers" n.d. http://pardam.cz/ (accessed July 17, 2017).

[63] c-m-p gmbh | products n.d. http://c-m-p-gmbh.de/products/ (accessed July 19, 2017).

[64] Molnar K, Vas L, Czigany T. Determination of tensile strength of electrospun single nanofibers through modeling tensile behavior of the nanofibrous mat. Compos Part B Eng 2012.

[65] Hiep NT, Lee B-T. Electro-spinning of PLGA/PCL blends for tissue engineering and their biocompatibility. J Mater Sci Mater Med 2010;21:1969–78. doi:10.1007/s10856-010-4048-y.

[66] Ghobadi S, Sadighikia S, Papila M, Cebeci FÇ, Gürsel SA. Graphene-reinforced

poly(vinyl alcohol) electrospun fibers as building blocks for high performance nanocomposites. RSC Adv 2015;5:85009–18. doi:10.1039/C5RA15689K.

[67] Menard K. Dynamic mechanical analysis: a practical introduction. 2008.

[68] Chandra R, Singh S, Gupta K. Damping studies in fiber-reinforced composites–a review. Compos Struct 1999.

[69] Ratna D. Epoxy composites: impact resistance and flame retardancy. 2007.

[70] Bilge K, Ürkmez A, Şimşek E, Papila M. Stabilized electrospinning of heat stimuli/ *in situ* crosslinkable nanofibers and their self-same nanocomposites. J Appl Polym Sci 2016;133. doi:10.1002/app.44090.

[71] Lubasova D, Martinova L. Controlled morphology of porous polyvinyl butyral nanofibers. J Nanomater 2011.

[72] Alzarrug FA, Stojanovic DB, Obradovic V, Kojovic A, Nedeljkovic JM, Rajilic-Stojanovic M, et al. Multiscale characterization of antimicrobial poly(vinyl butyral)/titania nanofibrous composites. Polym Adv Technol 2017;28:909–14. doi:10.1002/pat.3996.

[73] Stojanović DB, Zrilić M, Jančić-Heinemann R, Živković I, Kojović A, Uskoković PS, et al. Mechanical and anti-stabbing properties of modified thermoplastic polymers impregnated multiaxial *p* -aramid fabrics. Polym Adv Technol 2013;24:772–6. doi:10.1002/pat.3141.

[74] Obradovic V, STOJANOVIC D, Kojovic A. Electrospun Poly (vinylbutyral)/silica Composite Fibres for Impregnation of Aramid Fabrics. Materiale 2014.

[75] Miyasaka K, Ishikawa K. Effects of temperature and water on the $\gamma \rightarrow \alpha$ crystalline transition of nylon 6 caused by stretching in the chain direction. J Polym Sci Part A-2 Polym Phys 1968;6:1317–29.

doi:10.1002/pol.1968.160060709.

[76]   Wu T, Liao C. Polymorphism in nylon 6/clay nanocomposites. Macromol Chem Phys 2000.

[77]   Liu T, Yan S, Bonnet M, Lieberwirth I. DSC and TEM investigations on multiple melting phenomena in isotactic polystyrene. J Mater 2000.

[78]   Ji L, Zhang X. Ultrafine polyacrylonitrile/silica composite fibers via electrospinning. Mater Lett 2008.

[79]   Cassie A, Baxter S. Wettability of porous surfaces. Trans Faraday Soc 1944.

[80]   van der Heijden S. Study of nanofibre reinforced epoxy composites : curing behaviour and thermo-mechanical properties. - Master's thesis 2012.

[81]   Chen S, Hsu S-H, Wu M-C, Su WF. Kinetics studies on the accelerated curing of liquid crystalline epoxy resin/multiwalled carbon nanotube nanocomposites. J Polym Sci Part B Polym Phys 2011;49:301–9. doi:10.1002/polb.22179.

[82]   Hull D, Hull D, Hull D. topography CAMBRIDGE n.d.

[83]   Ashenai Ghasemi F, Ghorbani A, Ghasemi I. Mechanical, Thermal and Dynamic Mechanical Properties of PP/GF/xGnP Nanocomposites. Mech Compos Mater 2017;53:131–8. doi:10.1007/s11029-017-9647-y.

[84]   Toader G, Rusen E, Teodorescu M, Diacon A, Stanescu PO, Damian C, et al. New polyurea MWCNTs nanocomposite films with enhanced mechanical properties. J Appl Polym Sci 2017;134:45061. doi:10.1002/app.45061.

[85]   McAninch IM, Palmese GR, Lenhart JL, La Scala JJ. DMA testing of epoxy resins: The importance of dimensions. Polym Eng Sci 2015;55:2761–74. doi:10.1002/pen.24167.

[86]   Romo-Uribe A, Arizmendi L, Romero-Guzmán ME, Sepúlveda-Guzmán S,

Cruz-Silva R. Electrospun Nylon Nanofibers as Effective Reinforcement to Polyaniline Membranes. ACS Appl Mater Interfaces 2009;1:2502–8. doi:10.1021/am900456a.

[87] McAninch IM, Palmese GR, Lenhart JL, La Scala JJ. DMA testing of epoxy resins: The importance of dimensions. Polym Eng Sci 2015;55:2761–74. doi:10.1002/pen.24167.

[88] Chen L, Gong X, Li W. Effect of carbon black on the mechanical performances of magnetorheological elastomers. Polym Test 2008.

[89] Benveniste Y. A new approach to the application of Mori-Tanaka's theory in composite materials. Mech Mater 1987.

[90] Yao J, Bastiaansen C, Peijs T. High Strength and High Modulus Electrospun Nanofibers. Fibers 2014;2:158–86. doi:10.3390/fib2020158.

[91] Hang F, Lu D, Bailey RJ, Jimenez-Palomar I, Stachewicz U, Cortes-Ballesteros B, et al. *In situ* tensile testing of nanofibers by combining atomic force microscopy and scanning electron microscopy. Nanotechnology 2011;22:365708. doi:10.1088/0957-4484/22/36/365708.

[92] Finkel D. DIRECT optimization algorithm user guide. Cent Res Sci Comput North 2003.

[93] Dakota: Method Commands n.d. https://dakota.sandia.gov/sites/default/files/docs/5.4/html-ref/MethodCommands.html#MethodSCOLIBDIR (accessed July 22, 2017).